Eur. Phys. J. C (2011) 71:1737
DOI 10.1140/epjc/s10052-011-1737-8

THE EUROPEAN PHYSICAL JOURNAL C

Special Article - Tools for Experiment and Theory

Improved sensitivity to charged Higgs searches in top quark decays $t \to bH^+ \to b(\tau^+\nu_\tau)$ at the LHC using τ polarisation and multivariate techniques

Ahmed Ali[1,a], **Fernando Barreiro**[2,b], **Javier Llorente**[2,c]

[1]Deutsches Elektronen-Synchrotron DESY, 22607 Hamburg, Germany
[2]Facultad de Ciencias C-XI, Departamento de Fisica, Universidad Autonoma de Madrid (UAM), Cantoblanco, Madrid 28049, Spain

Received: 14 March 2011 / Revised: 7 July 2011 / Published online: 8 September 2011

Abstract We present an analysis with improved sensitivity to the light charged Higgs ($m_{H^+} < m_t - m_b$) searches in the top quark decays $t \to bH^+ \to b(\tau^+\nu_\tau) + \text{c.c.}$ in the $t\bar{t}$ and single $t/\bar{t}$ production processes at the LHC. In the Minimal Supersymmetric Standard Model (MSSM), one anticipates the branching ratio $\mathcal{B}(H^+ \to \tau^+\nu_\tau) \simeq 1$ over almost the entire allowed $\tan\beta$ range. Noting that the τ^+ arising from the decay $H^+ \to \tau^+\nu_\tau$ are predominantly right-polarized, as opposed to the τ^+ from the dominant background $W^+ \to \tau^+\nu_\tau$, which are left-polarized, a number of $H^+/W^+ \to \tau^+\nu_\tau$ discriminators have been proposed and studied in the literature. We consider hadronic decays of the $\tau^\pm$, concentrating on the dominant one-prong decay channel $\tau^\pm \to \rho^\pm\nu_\tau$. The energy and p_T of the charged prongs normalised to the corresponding quantities of the $\rho^\pm$ are convenient variables which serve as $\tau^\pm$ polariser. We use the distributions in these variables and several other kinematic quantities to train a boosted decision tree (BDT). Using the BDT classifier, and a variant of it called BDTD, which makes use of decorrelated variables, we have calculated the BDT(D)-response functions to estimate the signal efficiency vs. the rejection of the background. We argue that this chain of analysis has a high sensitivity to light charged Higgs searches up to a mass of 150 GeV in the decays $t \to bH^+$ (and charge conjugate) at the LHC. For the case of single top production, we also study the transverse mass of the system determined using Lagrange multipliers.

[a] e-mail: ahmed.ali@desy.de
[b] e-mail: fernando.barreiro@uam.es
[c] e-mail: Javier.Llorente.Merino@cern.ch

1 Introduction

In many extensions of the standard model (SM), the Higgs sector of the SM is enlarged by adding an extra doublet of complex Higgs fields. After spontaneous symmetry breaking, one finds three neutral Higgs bosons (h, H, A) and a pair of charged Higgs bosons, $H^\pm$. These neutral and charged Higgs bosons have been searched for in high energy experiments, in particular, at LEP and the Tevatron. None of these Higgses have been seen so far, and upper limits exist on all of them [1]. We will concentrate here on the charged Higgs searches, in which the two key phenomenological parameters are the charged Higgs mass, $m_{H^\pm}$, and $\tan\beta$, the ratio of the two vacuum expectation values, $\tan\beta = v_2/v_1$. The searches for the $H^\pm$ are model-dependent, and the exclusion limits (expressed as a contour in the $m_{H^\pm}$–$\tan\beta$ plane) have to be taken together with the underlying model. For example, in the so-called two-Higgs-doublet-models (2HDM), a stringent limit exists on $m_{H^\pm}$ from the measured branching ratio for $B \to X_s\gamma$ and the NNLO estimates of the same in the SM, yielding $m_{H^\pm} > 295(230)$ GeV at the 95% (99%) C.L., for almost the entire $\tan\beta$ values of interest [2]. This limit can be easily evaded in other models, in particular, in the minimal supersymmetric model (MSSM).

Direct $H^\pm$-searches are limited by the center-of-mass energy in $e^+e^- \to H^+H^-$ annihilation processes, where they can be produced via s-channel exchange of a photon or a Z boson. These searches assume for the branching ratios $\mathcal{B}(H^+ \to \tau^+\nu_\tau) + \mathcal{B}(H^+ \to c\bar{s}) = 1$ and hold for all values of $\mathcal{B}(H^+ \to \tau^+\nu_\tau)$. In the 2HDM framework, the cross section in the Born approximation depends only on $m_{H^\pm}$ (modulo the known couplings) and the present limit is $m_{H^\pm} > 79.3$ GeV at 95% C.L. obtained at $E_{\text{cm}}(e^+e^-) = 209$ GeV from LEP [1]. The mass range $m_{H^+} < m_t - m_b$ has been searched in the process $p\bar{p} \to t\bar{t}X$ at the Tevatron, followed by the decay $t \to bH^+$ (and its charge conjugate).

For example, Altonen et al. [3] have searched for the decay $t \to bH^+$, followed by $H^+ \to c\bar{s}$ in 2.2 fb^{-1} of $p\bar{p}$ collisions at $E_{\rm cm}(p\bar{p}) = 1.96$ TeV, obtaining upper limits on $\mathcal{B}(t \to bH^+)$ between 0.08 and 0.32 (95% C.L.), assuming $\mathcal{B}(H^+ \to c\bar{s}) = 1$. In the MSSM, this probes only a very small $\tan\beta$ region, namely $\beta < 1$, which is not favoured by theoretical considerations [4]. The search for $t \to bH^+$, followed by $H^+ \to \tau^+\nu_\tau$ by Abazov et al. [5] in 0.9^{-1} of $p\bar{p}$ collisions at the Tevatron yield upper limits on $\mathcal{B}(t \to bH^+)$ between 0.19 and 0.25 (95% C.L.) for $m_{H^+} = 80$–155 GeV and $\mathcal{B}(H^+ \to \tau^+\nu_\tau) = 1$. This excludes a small region ($\tan\beta > 35$ and $m_{H^+} = 100$–120 GeV) [6]. Thus, it is fair to conclude that the searches of the charged Higgses over a good part of the $m_{H^\pm}$–$\tan\beta$ plane in the MSSM is a programme that still has to be carried out and this belongs to the LHC experiments. In anticipation, searches for the $H^\pm$ in pp collisions at $E_{\rm cm} = 7$–14 TeV at the LHC have received a lot of attention [7–12]. There are two regions, namely $m_{H^+} < m_t - m_b$, which will be looked into in both the $t\bar{t}$ pair production and in single top (or anti-top) production in pp collisions, followed by the decays $t \to bH^+$ and $H^+ \to \tau^+\nu_\tau$, and for $m_{H^\pm}$ above the top quark mass, in which case $H^\pm$ production mainly takes place through the process $gb \to tH^+$, followed dominantly by the decay $H^+ \to t\bar{b}$. However, despite larger branching fraction, it may be hard to distinguish the $H^+ \to t\bar{b}$ mode from the background. For large $\tan\beta$, the decay mode $H^+ \to \tau^+\nu_\tau$ becomes discernible. In this paper, we will concentrate on the light $H^\pm$-scenario.

The decay channel $H^\pm \to \tau^\pm + \nu_\tau$ will play the key role in the searches of the light $H^\pm$-bosons. The τ^+ leptons arising from the decays $W^+ \to \tau^+\nu_\tau$ and $H^+ \to \tau^+\nu_\tau$ are predominantly left- and right-polarised, respectively. Polarisation of the $\tau^\pm$ influences the energy distributions in the subsequent decays of the $\tau^\pm$. Strategies to enhance the $H^\pm$-induced effects in the decay $t \to b(W^+, H^+) \to b(\tau^+\nu_\tau)$, based on the polarisation of the τ^+ have been discussed at length, starting from the pioneering work [13–16] to the production and decays of a $t\bar{t}$ pair at the hadron colliders Tevatron and the LHC [17–22]. Also the effects of the (QED and QCD) radiative corrections on such distributions in the dominant (one-charged prong) decay channels $\tau^+ \to \pi^+\nu_\tau, \rho^+\nu_\tau, a_1^+\nu_\tau$ and $\ell^+\bar{\nu}_\ell\nu_\tau$ have been worked out [23]. Following these studies, the construction of the $\tau^\pm$-jet (as well as b-jet) are of central importance in $H^\pm$-searches. We use the dominant single-charged-prong decay $\tau^\pm \to \rho^\pm\nu_\tau$ as the $\tau^\pm$ polariser. As $\rho^\pm \to \pi^\pm\pi^0$ is the dominant decay mode, the energy and transverse momentum of the $\pi^\pm$ in the $\tau^\pm$-jet become quantities of main interest for our study. Likewise, the distribution in the angle ψ, defined as

$$\cos\psi = \frac{2m^2_{\rho b}}{m^2_{\rm top} - m^2_W} - 1, \tag{1}$$

plays an important role in our analysis. Since the energy-momentum vectors of the b-jet and the $\rho^\pm$ can be measured, this distribution is measurable at the LHC. We also note that this distribution is different from the conventional definition of the angle ψ [24], in which the invariant mass $m^2_{\ell b}$ is measured instead of $m^2_{\rho b}$. The other distributions that enter in our analysis are listed in the next section.

Having generated these distributions, characterising the signal $t \to bH^+ \to b(\tau^+\nu_\tau) \to b(\rho^+\bar{\nu}_\tau)\nu_\tau$ and the background $t \to bW^+ \to b(\tau^+\nu_\tau) \to b(\rho^+\bar{\nu}_\tau)\nu_\tau$ events, we use a technique called the Boosted Decision Tree (BDT)—a classification model used widely in data mining [25]—to develop an identifier optimised for the $t \to bH^+$ decays. In our calculation, we use both BDT and a variant of it called BDTD (here D stands for decorrelated), where possible correlations in the input variables are removed by a proper rotation obtained from the decomposition of the square root of the covariance matrix, to discriminate the signal events from the large backgrounds. We recall that this technique has been successfully used to establish the single top quark production in $p\bar{p}$ collisions at the Tevatron [26, 27] (see [28] for details). Recently, we have applied this technique to a feasibility study of measuring the CKM matrix element $|V_{ts}|$ from the decay $t \to Ws$ at the LHC@14 TeV, and have estimated that a benchmark with 10% accuracy for this decay mode with a 10^3 rejection of the background $t \to Wb$ can be achieved with an integrated luminosity of 10 (fb)$^{-1}$ [29]. We show in this paper that a similar BDTD-based analysis holds great promise in light-$H^\pm$ searches at the LHC both in the $pp \to t\bar{t}X$ pair production and in the single top (or anti-top) production $pp \to t/\bar{t}X$. Furthermore, we show that using a transverse mass definition, as suggested in [30], the process $pp \to t/\bar{t}X$ followed by the decays $t \to bH^+, bW^+$, allows one to determine rather sharp Jacobian peaks for the transverse mass of the $H^\pm$-bosons. The conventional definition of the transverse mass [31], which was very helpful in the determination of the transverse mass of the $W^\pm$ bosons, is less suited for constructing the corresponding mass of the $H^\pm$ bosons.

We note that an analysis using an iterative discriminant analysis method similar to the one presented here was carried out by Hesselbach et al. [32]. In particular, detailed Monte Carlo comparisons of several variables incorporating the spin effects in charged Higgs boson production were presented to separate the tbH^+ signal from the standard model $t\bar{t}$ background both at the Tevatron ($\sqrt{s} = 1.96$ TeV) and the LHC ($\sqrt{s} = 14$ TeV). However, there are several significant differences in the two studies, such as the distribution in $\cos\psi$ (defined in (1)), which plays an important role in our analysis. In addition, we have studied the case of single top production at the LHC, $pp \to t/\bar{t} + X$, followed by the decays $t \to b(H^+/W^+ \to \tau^+\nu_\tau) + \text{c.c.}$, which was not considered in [32].

This paper is organised as follows: In Sect. 2, we analyse the process $pp \to t\bar{t}X$ at the LHC, followed by the decay chains $t \to bW^+, bH^+$, and the subsequent decays $(H^+, W^+) \to \tau^+\nu_\tau$, together with the BDTD-based analysis of the signal $(t \to bH^+)$ and the SM decay background $(t \to bW^+)$. The BDTD response functions are then used to work out the signal efficiency vs. the background rejection. In Sect. 3, we repeat this analysis for the single top (or anti-top) production $pp \to t/\bar{t}X$ at the LHC. Section 4 contains a brief summary.

2 $t\bar{t}$ production and the decay chains $t \to bW^+/H^+ \to b(\tau^+\nu_\tau)$ at the LHC

2.1 Production cross sections

Theoretical predictions of the top quark production at the LHC have been obtained by including up to the next-to-next-to-leading order (NNLO) corrections in the strong coupling constant [33–36] using modern parton distribution functions (PDFs) [37, 38]. Typical estimates for $\sigma(pp \to t\bar{t}X)$ range from 874^{+14}_{-33} pb for $m_t = 173$ GeV and $\sqrt{s} = 14$ TeV [39] to $943 \pm 4(\text{kinematics})^{+77}_{-49}(\text{scale}) \pm 12(\text{PDF})$ pb [35]. Compared to the $t\bar{t}$ production cross section at the Tevatron, this is larger by two orders of magnitude. The cross sections at the lower LHC energies, 7 and 10 TeV, have also been calculated [35, 39], with $\sigma(pp \to t\bar{t}X) \simeq 400$ pb at 10 TeV and about half that number at 7 TeV. Thus, for the top quark physics, the dividends in going from 7 to 14 TeV are higher by a good factor 4.

2.2 Top quark decays $t \to b(W^+, H^+)$ and charged Higgs decays $H^+ \to c\bar{s}, \tau^+\nu_\tau$

Top-quark decays within the Standard Model are completely dominated by the mode

$$t \to b + W^+, \tag{2}$$

due to $V_{tb} = 1$ to a very high accuracy. In beyond-the-SM theories with an extended Higgs sector, a light charged Higgs can also be produced via

$$t \to b + H^+. \tag{3}$$

The relevant part of the interaction Lagrangian is [18, 19]:

$$\begin{aligned}\mathcal{L}_I = {} & \frac{g}{2\sqrt{2}M_W} V_{tb} H^+ \left[\bar{u}_t(p_t)\left\{A(1+\gamma_5)\right.\right. \\ & \left.\left. + B(1-\gamma_5)\right\} u_b(p_b)\right] \\ & + \frac{gC}{2\sqrt{2}M_W} H^+ \left[\bar{u}_{\nu_l}(p_\nu)(1-\gamma_5)u_l(p_l)\right],\end{aligned} \tag{4}$$

where A, B and C are model-dependent parameters which depend on the fermion masses and $\tan\beta$:

$$A = m_t \cot\beta, \qquad B = m_b \tan\beta, \qquad C = m_\tau \tan\beta. \tag{5}$$

The decay widths of processes (2) and (3) in the Born approximation are [18, 19]:

$$\begin{aligned}\Gamma^{\text{Born}}_{t\to bW} = {} & \frac{g^2}{64\pi M_W^2 m_t} \lambda^{\frac{1}{2}}\left(1, \frac{m_b^2}{m_t^2}, \frac{M_W^2}{m_t^2}\right) \\ & \times\left[M_W^2\left(m_t^2 + m_b^2\right) + \left(m_t^2 - m_b^2\right)^2 - 2M_W^4\right],\end{aligned} \tag{6}$$

$$\begin{aligned}\Gamma^{\text{Born}}_{t\to bH} = {} & \frac{g^2}{64\pi M_W^2 m_t} \lambda^{\frac{1}{2}}\left(1, \frac{m_b^2}{m_t^2}, \frac{M_H^2}{m_t^2}\right) \\ & \times\left[\left(m_t^2\cot^2\beta + m_b^2\tan^2\beta\right)\left(m_t^2 + m_b^2 - M_H^2\right)\right. \\ & \left. - 4m_t^2 m_b^2\right],\end{aligned} \tag{7}$$

where $\lambda(x, y, z) = x^2 + y^2 + z^2 - 2xy - 2xz - 2yz$ is the triangle function. The total top quark decay width in the Born approximation is obtained by adding the two partial widths

$$\Gamma_t^{\text{tot, Born}} = \Gamma^{\text{Born}}_{t\to bW} + \Gamma^{\text{Born}}_{t\to bH}. \tag{8}$$

QED corrections in the total decay width of the top quark are numerically small. The $O(\alpha_s)$ QCD corrections were calculated in [40, 41] (see, also [42]) and have the form:

$$\begin{aligned}\Gamma^{\text{tot}}_{t,RC} &= \Gamma^{\text{Born+QCD}}_{t\to bW} + \Gamma^{\text{Born+QCD}}_{t\to bH}, \\ \Gamma^{\text{Born+QCD}}_{t\to b(W,H)} &= \Gamma_t^{\text{tot,Born}}\left(1 + f_{W,H}\right), \\ f_{W,H} &= \frac{\alpha_s}{3\pi}\left(5 - \frac{4\pi^2}{3}\right).\end{aligned} \tag{9}$$

Thus, in the branching ratio $\mathcal{B}(t \to bH^+)$, also this QCD correction drops out. However, radiative corrections coming from the supersymmetric sector to $\mathcal{B}(t \to bH^+)$ are rather important. They have been calculated in great detail in the literature, in particular for the MSSM scenario in [43–45], and can be effectively incorporated by replacing the b-quark mass m_b in the Lagrangian for the decay $t \to bH^+$ by the SUSY-corrected mass $m_b^{\text{corrected}} = m_b/[1 + \Delta_b]$. The correction Δ_b is a function of the supersymmetric parameters and, for given MSSM scenarios, this can be calculated using the FeynHiggs programme [46]. In particular, for large values of $\tan\beta$ (say, $\tan\beta > 20$), the MSSM corrections increase the branching ratio for $t \to bH^+$ significantly. This, for example, can be seen in a particular MSSM scenario in a recent update [47], from where we show $\mathcal{B}(t \to bH^+)$ as a function of $\tan\beta$, calculated for $m_t = 175$ GeV and various assumed values of the charged Higgs mass, indicated in Fig. 1.

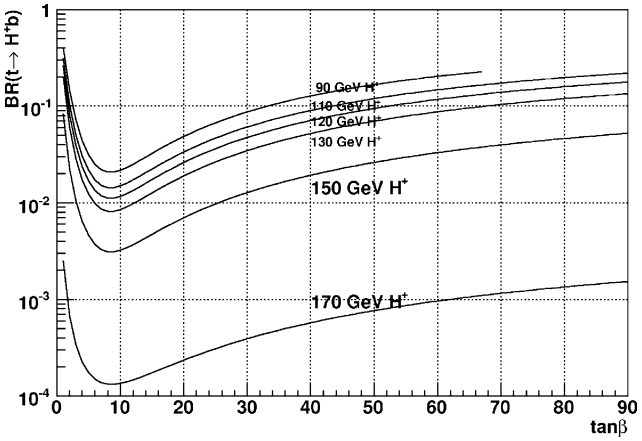

Fig. 1 Branching ratio $\mathcal{B}(t \to H^+ b)$ in MSSM as a function of $\tan\beta$ for the charged Higgs masses as indicated. (Figure taken from [47])

Since we are treating the case of the light charged Higgs, there are essentially only two decay modes which are important: $H^+ \to \tau^+ \nu_\tau$ and $H^+ \to c\bar{s}$. The branching ratio of interest to us $\mathcal{B}(H^+ \to \tau^+ \nu_\tau)$ is given by [18, 19]:

$$\begin{aligned}
\mathcal{B}\big(H^+ \to \tau^+ \nu_\tau\big) &= \frac{\Gamma_{H\to\tau\nu_\tau}}{\Gamma_{H\to\tau\nu_\tau} + \Gamma_{H\to c\bar{s}}}, \\
\Gamma_{H\to\tau\nu_\tau} &= \frac{g^2 M_H}{32\pi M_W^2} m_\tau^2 \tan^2\beta, \\
\Gamma_{H\to c\bar{s}} &= \frac{3g^2 M_H}{32\pi M_W^2}\big(m_c^2 \cot^2\beta + m_s^2 \tan^2\beta\big).
\end{aligned} \tag{10}$$

For the numerical values of $\tan\beta$ that we entertain in this paper, the branching ratio $\mathcal{B}(H^+ \to \tau^+ \nu_\tau) = 1$, to a very high accuracy.

2.3 Event generation, trigger

We consider in this section the process $pp \to t\bar{t}X$, with both the t and $\bar{t}$ decaying into Wb. Our trigger is the leptonic decay $W^- \to e^- \bar{\nu}_e$ or $W^- \to \mu^- \bar{\nu}_\mu$. The other W^+ decays via $W^+ \to \tau^+ \nu_\tau$. This makes up our main background. The signal events are generated in which one of the t or $\bar{t}$ decays via $W^+ \to bH^+$ (or its charge conjugate $W^- \to bH^-$), see Fig. 2. The other $\bar{t}$ or t then decays leptonically, as in our trigger. In the Minimal Supersymmetric Standard Model (MSSM), for large $\tan\beta$ and $m_{H^+} < m_t$, the branching ratio for the decay $H^+ \to c\bar{s}$ is small and one anticipates the branching ratio $\mathcal{B}(H^+ \to \tau^+ \nu_\tau) \simeq 1$. This is the parameter space in which the analysis reported here is valid. Noting that the τ^+ arising from the decay $H^+ \to \tau^+ \nu_\tau$ are predominantly right-polarized, as opposed to the τ^+ from the dominant background $W^+ \to \tau^+ \nu_\tau$, which are left-polarized, a number of $H^+/W^+ \to \tau^+ \nu_\tau$ discriminators have been proposed and studied in the literature. We have used the dominant single-charged-prong decay $\tau^+ \to \rho^+ \nu_\tau$ as the

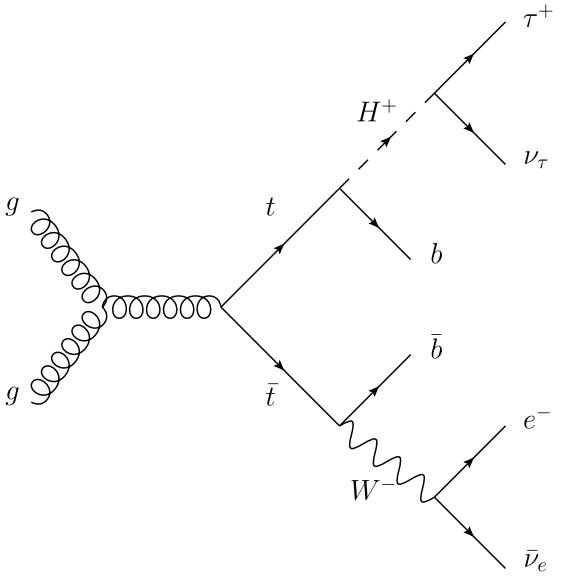

Fig. 2 Feynman diagram for $gg \to t\bar{t}$, followed by the decay $t \to b(H^+ \to \tau^+ \nu_\tau)$ and $\bar{t} \to \bar{b}(W^- \to e^- \bar{\nu}_e)$

τ^+ polariser. Having set these branchings, we have generated 50K events for the process $pp \to t\bar{t} \to bW^+(\bar{b}W^-)$, with all of them decaying according to the chain described earlier, i.e., $W^- \to e^- \nu_e$ and $W^+ \to \tau^+ \nu_\tau$, with all the τ's forced to decay into $\rho + \nu_\tau$ (here and below, charge conjugates are implied). In calculating the required luminosity, we take into account the corresponding branching ratios, which are as follows [1]

$$\begin{aligned}
&\mathcal{B}\big(W^+ \to e^+ \nu_e\big) = (10.75 \pm 0.13)\%, \\
&\mathcal{B}\big(W^+ \to \tau^+ \nu_\tau\big) = (11.25 \pm 0.20)\%, \\
&\mathcal{B}\big(H^+ \to \tau^+ \nu_\tau\big) = 1.0, \\
&\mathcal{B}\big(\tau^+ \to \rho^+ \nu_\tau\big) = (25.5 \pm 0.10)\%.
\end{aligned} \tag{11}$$

We also generate the same number (50K) signal events, for each of the following charged Higgs masses: $m_{H^+} = 90, 110, 130, 150$ GeV. As for the background process, we force the τ^+ to decay into $\rho^+ \nu_\tau$ 100% of the time. These events are generated using PYTHIA 6.4 [48] and for the decays of the $\tau^\pm$, we use the programme called TAUOLA [49] to incorporate the $\tau^\pm$ polarization information on the decay distributions.

We impose the following acceptance and trigger cuts:

- $|\eta_\ell| < 2.5$, with $\ell = e, \tau$
- $|\eta_{b,\bar{b}}| < 2.5$
- $P_{T_e} > 20$ GeV
- $P_{T_\rho} > 10$ GeV
- $P_{T_{b,\bar{b}}} > 20$ GeV

In order to discriminate the signal and background, we have studied a number of distributions, summarized below.

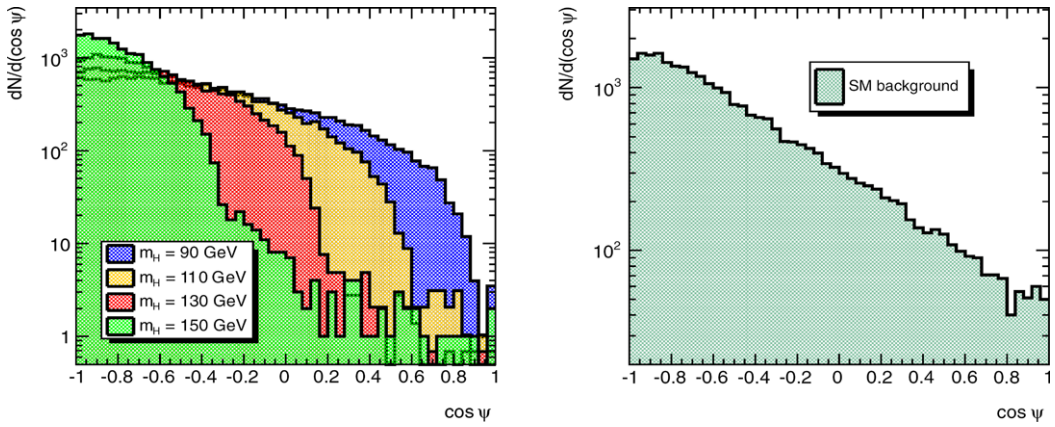

Fig. 3 (Color online) The distribution $dN/d\cos\psi$ for the $t\bar{t}$ production as measured in the decay chain $t \to bW \to b(\tau\nu_\tau) \to b(\rho\bar{\nu}_\tau)\nu_\tau)$ (*right-hand frame*), and in $t \to bH \to b(\tau\nu_\tau) \to b(\rho\bar{\nu}_\tau)\nu_\tau)$ for four different charged Higgs masses, as indicated on the figure (*left-hand frame*)

- Distribution in the angle ψ, defined in (1). This is defined for both the decay chains: $t \to bW \to b(\tau\nu_\tau) \to b(\rho\bar{\nu}_\tau)\nu_\tau$ and $t \to bH \to b(\tau\nu_\tau) \to b(\rho\bar{\nu}_\tau)\nu_\tau$. Since the energy-momentum vectors of the b-jet and the $\rho^\pm$ can be measured, this distribution is measurable at the LHC. We also note that this distribution is different from the conventional definition of the angle ψ [24], in which the invariant mass $m^2_{\ell b}$ is measured instead of $m^2_{\rho b}$.
- Energy and p_T of the b-jets from the decays $t \to bW^+$ and $t \to bH^+$.
- Energy and p_T of the τ^+ jets from the decays $W^+ \to \tau^+\nu_\tau$ and $H^+ \to \tau^+\nu_\tau$, concentrating on the single-charged-prong decays $\tau^+ \to \rho^+\nu_\tau$.
- The ratio of the energy and p_T of the τ^+ jets and their accompanying b-jet.
- As a measure of the τ polarisation, we consider the fractional energy and transverse momentum of the single-charged prong (π^+ in τ^+-jet).
- For the case of single top production, we also study the transverse mass of the system determined using Lagrange multipliers [30].
- These distributions are used to train a boosted decision tree (BDT). Using the BDT classifier, and a variant of it called BDTD, which makes use of decorrelated variables, we have calculated the BDT(D)-response functions to estimate the signal efficiency vs. the rejection of the background.

The strategy adopted by us to search for the decays $t \to bH^+$ is somewhat different from the traditional cut-based analysis, as, for example, reported in [8]. There the idea is to suppress the SM-background as much as possible, making use of additional variables, such as the missing E_T, satisfying $E_T^{\rm miss} > 50$ GeV. Our idea is, instead, to train a boosted decision tree classifier for both the signal and background events. Eventually, for a realistic analysis of the LHC data, we may have to reintroduce some of the cuts to suppress other non-$t\bar{t}$ background, such as coming from the process $pp \to W^\pm +$ jets, which may also fake our signal.

2.4 Details of the analysis

In Fig. 3 (right-hand frame), we show the $\cos\psi$ distributions for the standard model (SM) process $p + p \to t\bar{t} + X$, followed by the decay chain $t \to bW \to b(\tau\nu_\tau) \to b(\rho\bar{\nu}_\tau)\nu_\tau$. In the left-hand frame, we show the same distribution when one of the t or $\bar{t}$ decays via the chain $t \to bH \to b(\tau\nu_\tau) \to b(\rho\bar{\nu}_\tau)\nu_\tau$, for four different charged Higgs masses, as already stated in the previous section. For lower values of m_{H^+}, the $\cos\psi$ distribution falls less steeply than the SM background. As m_{H^+} increases, the $\cos\psi$ distributions become steeper and are essentially confined to the negative values of $\cos\psi$. This distribution then provides one of the discriminators to be fed to the BDTD analysis.

In Fig. 4 (right-hand frames), we show the distributions in the energy of the b-jet, $E(b)$, and the transverse momentum of the b-jet, $p_T(b)$ from the SM process $pp \to t\bar{t}X$, followed by the decay chain discussed above. In the left-hand frames, the corresponding distributions are shown for the charged Higgs case. We remark that for the charged Higgs case these distributions are softer than those from the SM due to the different helicity structure of the decays. This effect becomes stronger as m_{H^+} increases due to phase space. As a result, these distributions add to the discrimination power of the BDTD analysis. Note that these distributions reflect the event characteristics at the generation level. Obviously, due to the semileptonic decays of the b-quark, and other detector effects, they will be modified. However, we expect that the dilutions due to these effects are subdominant.

In Fig. 5 (right-hand frames), we show the distributions in the energy of the τ-jet, $E(\tau\text{-jet})$, and in the transverse

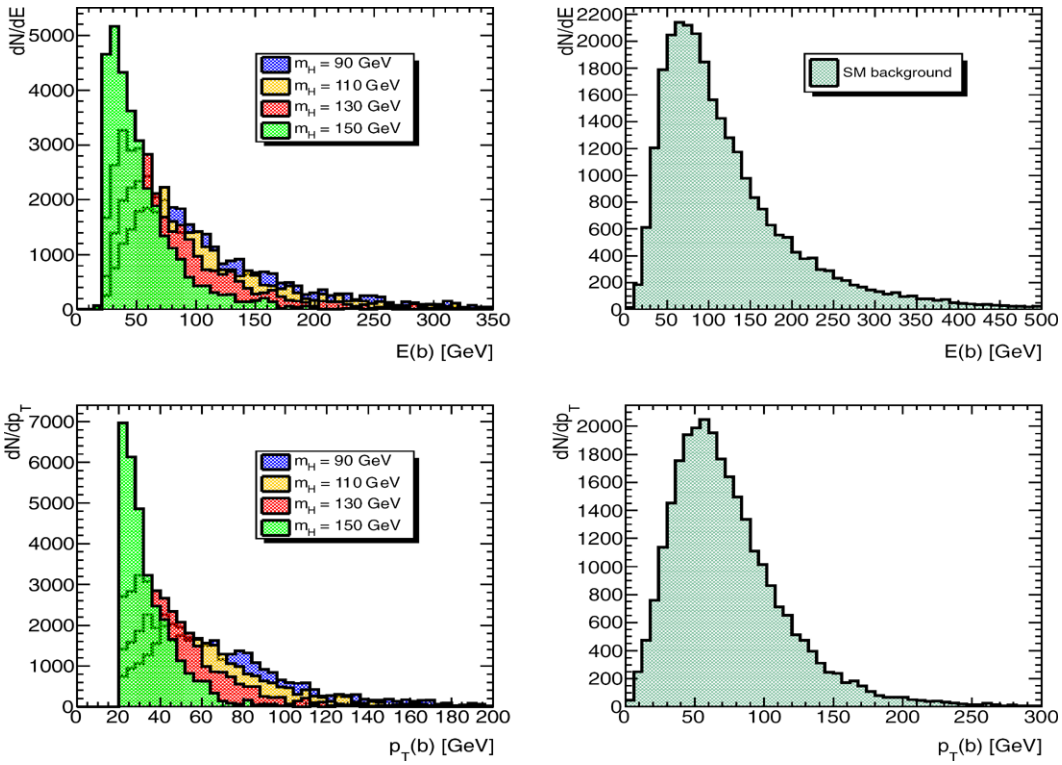

Fig. 4 (Color online) Distributions in the Energy of the b-jet, $E(b)$, and transverse momentum of the b-jet, $p_T(b)$ from the process $pp \to t\bar{t}X$, followed by the decay $t \to W^+b$ (*right-hand frames*), and the same distributions for the decay chain $t \to H^+b$ with the four indicated charged Higgs masses (*left-hand frame*)

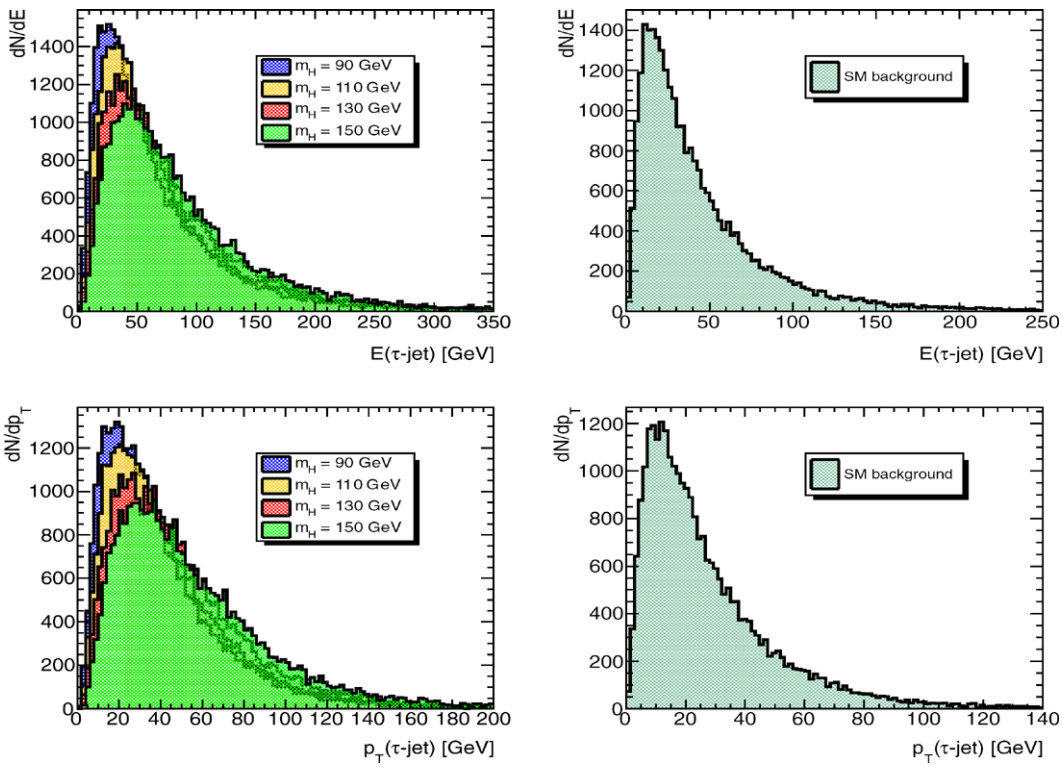

Fig. 5 (Color online) Distributions in the Energy of the τ-jet, $E(\tau\text{-jet})$, and transverse momentum of the τ-jet, $p_T(\tau\text{-jet})$ from the process $pp \to t\bar{t}X$, followed by the decay $t \to W^+b$ (*right-hand frames*), and the same distributions for the decay chain $t \to H^+b$ with the four indicated charged Higgs masses (*left-hand frame*)

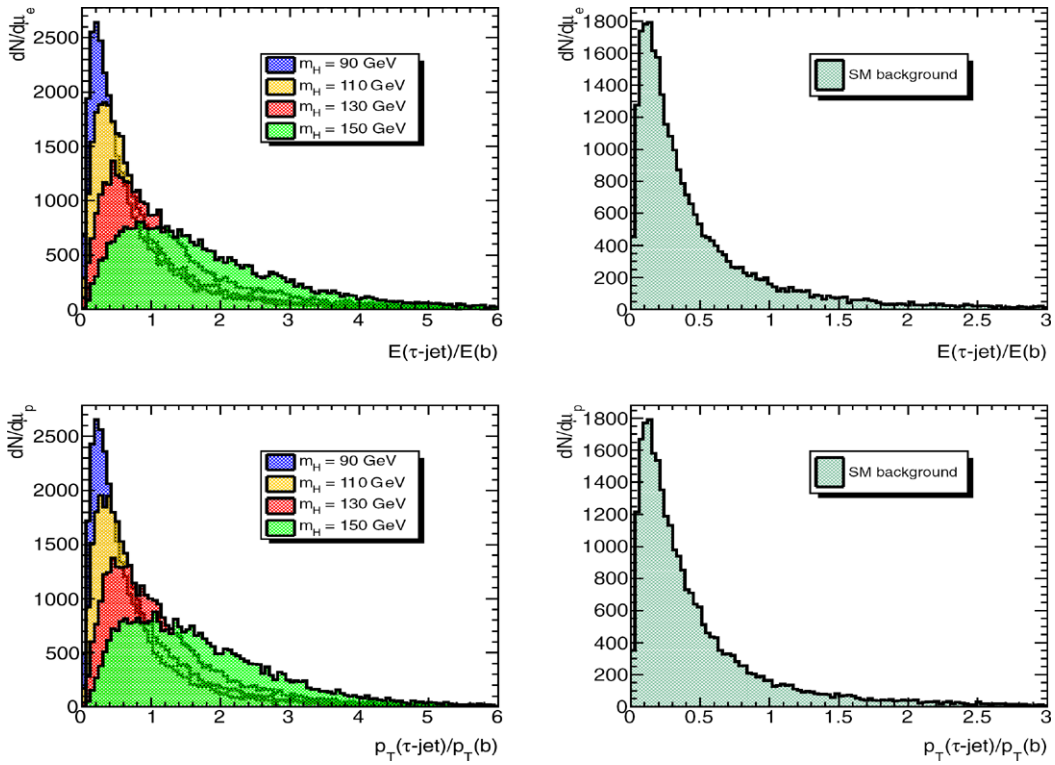

Fig. 6 (Color online) Distributions in the ratio $E(\tau\text{-jet})/E(b)$ and $p_T(\tau\text{-jet})/p_T(b)$ from the process $pp \to t\bar{t}X$, followed by the decay $t \to W^+b$ (*right-hand frames*), and the same distributions for the decay chain $t \to H^+b$ with the four indicated charged Higgs masses (*left-hand frame*)

momentum of the τ-jet, $p_T(\tau\text{-jet})$ from the SM process, followed by the decay chain discussed above. In the left-hand frames, the corresponding distributions are shown for the charged Higgs case. In these distributions, the energy and p_T-spectra of the τ-jet coming from the charged Higgs decays are harder than those coming from the SM process, and this difference becomes more marked as m_{H^+} increases. This complementary behaviour is expected for the same reason as discussed earlier for Fig. 4, again reflecting the differences in helicity and phase space. It goes without saying that these distributions increase the discrimination power of the BDTD analysis.

To make this effect more marked, we show the ratio of the energy and p_T-spectra involving the τ- and b-jets in Fig. 6. The SM distributions are shown in the right-hand frames, and those from the charged Higgs in the left-hand frames. These distributions show clearly the different shapes of the distributions SM vs. Higgs. For example, putting a lower cut on the ratios $E(\tau\text{-jet})/E(b) > 1$ or $p_T(\tau\text{-jet})/p_T(b) > 1$, most of the SM background is eliminated, whereas the charged Higgs-induced distributions surviving this cut are considerably larger, with the discrimination becoming stronger as m_{H^+} increases.

In Fig. 7, we show the distributions in the fractional energy of the single-charged prong (π^+ in τ^+-jet), $E(\pi)/E(\tau\text{-jet})$, and in the transverse momentum of the single-charged prong, $p_T(\pi)/p_T(\tau\text{-jet})$ from the SM process (right-hand frames) and those coming from the charged Higgs-induced process (left-hand frames) for $m_{H^+} = 90$ GeV. As remarked earlier, we are using the dominant single-charged-prong decay $\tau^+ \to \rho^+\bar{\nu}_\tau$ as the τ^+ polariser. As already noted in [14], the fractional energy distributions in $z = E_A/E_\tau$, from the τ-decay products $\tau \to A+$ missing energy, the effect of the $\tau^\pm$ polarization is most marked for the decays $\tau^+ \to \pi^+\bar{\nu}_\tau$ and $\tau^+ \to \rho^+\bar{\nu}_\tau$. This has been worked out in the collinear limit, i.e., for $E_\tau/m_\tau \gg 1$. Our variables differ from the one used in [14], in that we normalize to the visible τ-energy and the visible $p_T(\tau\text{-jet})$, and not to the total τ-energy. With our normalization, the π^+-energy measured in the decays $\tau^+ \to \pi^+\bar{\nu}_\tau$ will be a delta function, peaked at 1 in the variables shown in Fig. 7, and hence we concentrate on the decay chain $\tau^+ \to \rho^+\bar{\nu}_\tau$. These distributions also provide strong discriminants for the BDTD analysis.

Briefly, the generated input is used for the purpose of training and testing the samples. We provide the input in terms of the variables discussed earlier for the signal ($t \to bH^+$) and the background ($t \to bW^+$), obtained with the help of a Monte Carlo generator. This information is used to develop the splitting criteria to determine the best partitions of the data into signal and background to build up a decision tree (DT). The separation algorithm used in splitting the group of events in building up DT plays an impor-

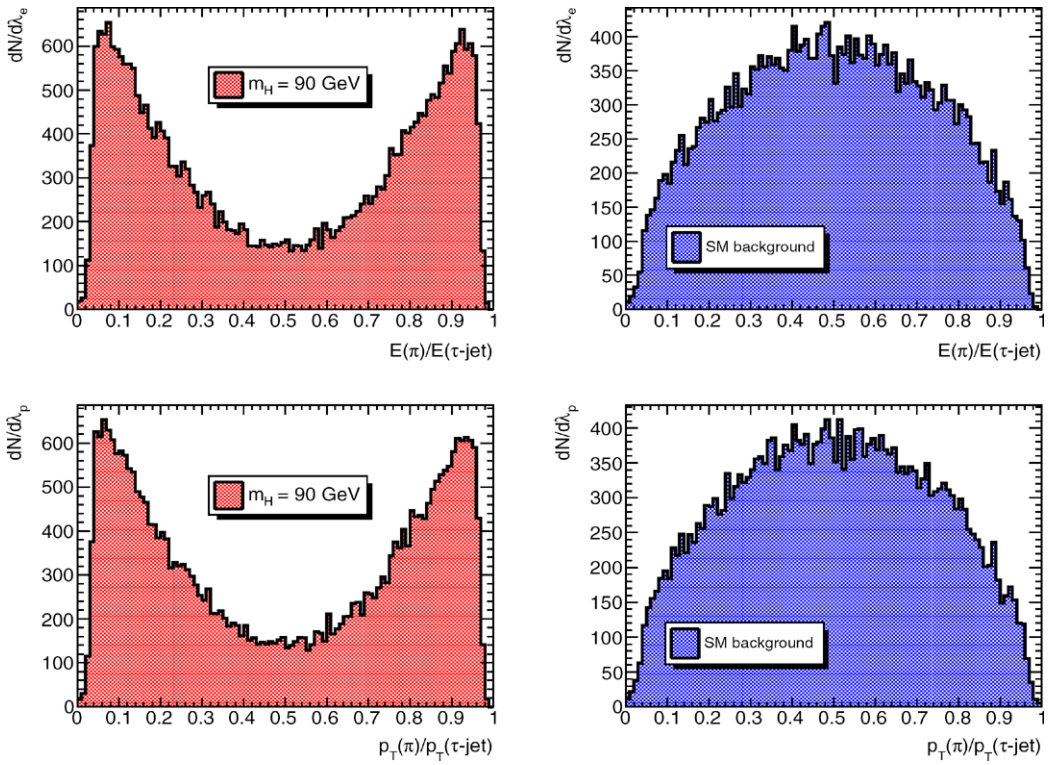

Fig. 7 (Color online) Distributions in the fractional energy of the single-charged prong (π^+ in τ^+-jet), $E(\pi)/E(\tau\text{-jet})$, and in the transverse momentum of the single-charged prong, $p_T(\pi)/p_T(\tau\text{-jet})$ from the $pp \to t\bar{t}X$, followed by the decay $t \to W^+b$ (*right-hand frames*), and the same distributions for the decay chain $t \to H^+b$ with the four indicated charged Higgs masses (*left-hand frame*)

tant role in the performance. The software called the Toolkit for Multivariate Data Analysis in ROOT (TMVA) [50] is used for the BDT(D) responses in our analysis. The response functions for $pp \to t\bar{t}X$ at a center-of-mass-energy $\sqrt{s} = 14$ TeV at the LHC, followed by the background process $t \to bW^+$ (in shaded blue) and the signal $t \to bH^+$ (in shaded red) are shown in Fig. 8. The four frames shown in this figure correspond to the charged Higgs masses $m_{H^+} =$ 90, 110, 130 and 150 GeV. As can be seen that the separation between the signal and the background increases as m_{H^+} increases. This improved separation as a function of m_{H^+} will, however, be compensated to some extent by the decreasing branching ratio for the decay $t \to bH^+$, as shown in Fig. 1 [47], obtained by using FeynHiggs [51].

The corresponding background rejection vs. signal efficiency curves from the process $pp \to t\bar{t}X$ calculated from the previous BDTD response at $\sqrt{s} = 14$ TeV are shown in Fig. 9 for the four charged Higgs masses, as indicated on the frames. For a signal efficiency value of 90%, the background rejection varies between 50% and 90% as we move from $m_{H^+} = 90$ GeV to $m_{H^+} = 150$ GeV.

In order to calculate the significance of our signal, we do the following simplified calculation. We consider the less preferred case for $\tan\beta = 10$, for which the branching ratio $\mathcal{B}(t \to H^+b)$ in the MSSM shows a dip, with $\mathcal{B}(t \to H^+b) \simeq 0.02$ for $m_{H^+} = 90$ GeV (see, Fig. 1). For the process $pp \to t\bar{t}X$, the trigger is based on the decay $t \to bW^+ \to b\ell^+\nu_\ell$, with $\ell^+ = e^+, \mu^+$, which has a summed branching ratio of about 0.2. Since, in the large-tan β limit we are working, $\mathcal{B}(H^+ \to \tau^+\nu_\tau) \simeq 1$, and the τ^+-decay mode we are concentrating on is $\tau^+ \to \rho^+\bar{\nu}_\tau$, which has a branching ratio of 0.25, the product branching ratio $t \to bH^+ \to b(\tau^+\nu_\tau) \to b(\rho^+\bar{\nu}_\tau)\nu_\tau = 5 \times 10^{-3}$, which taking into account the trigger is reduced to 1.0×10^{-3}. For an integrated luminosity of 10 (fb)$^{-1}$ at $\sqrt{s} = 14$ TeV, and summing over the charge conjugated modes yielding a factor 2, this yields 2×10^4 signal events. For the background events, resulting from the production and the SM decays from the process $pp \to t\bar{t}X$, the corresponding product branching ratio is 2.5%, which together with the trigger branching gives 5×10^{-3}, resulting in 10^5 background events, where we have again taken into account the factor 2 from the sum of the charge conjugated states. Using the BDTD analysis, we get for a 50% signal efficiency, a background rejection of 90%. Thus, our estimated significance will be

$$S = \frac{N_{\text{signal events}}}{\sqrt{N_{\text{background events}}}} = \frac{10^4}{\sqrt{10^4}} \simeq 100. \tag{12}$$

A more realistic calculation should consider a factor of 2 reduction due to the acceptance cuts, discussed in Sect. 2.3,

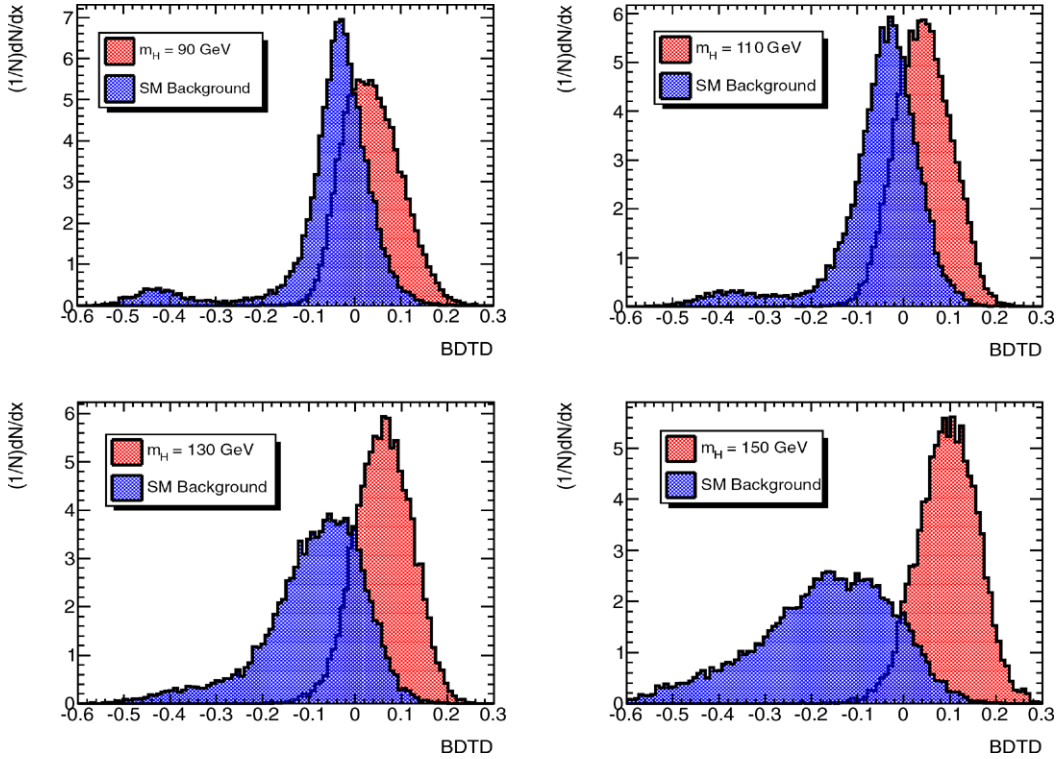

Fig. 8 (Color online) BDTD response functions for $pp \to t\bar{t}X$, with $\sqrt{s} = 14$ TeV, followed by the decay $t \to W^+b$ (SM) and the decay chain $t \to H^+b$, with the SM background (in *shaded blue*) and the charged Higgs signal process (in *shaded red*) for four different charged Higgs masses

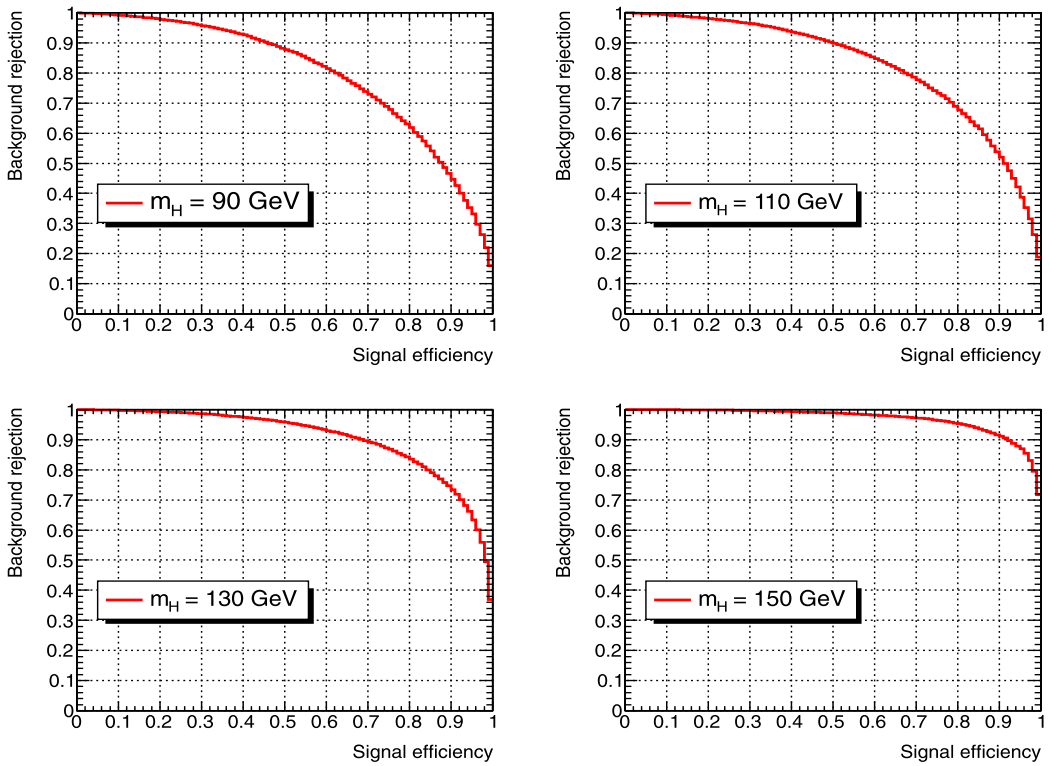

Fig. 9 (Color online) SM background rejection vs. charged Higgs signal efficiency for the four charged Higgs masses indicated on the figure from the process $pp \to t\bar{t}X$, with $\sqrt{s} = 14$ TeV

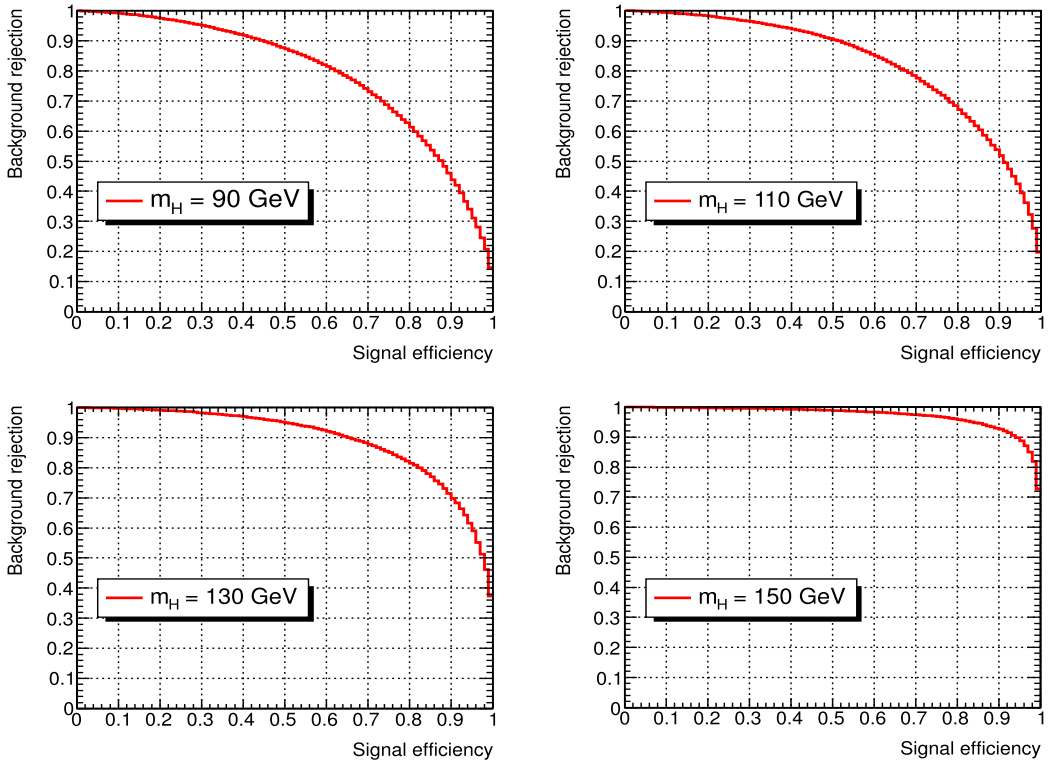

Fig. 10 (Color online) SM background rejection vs. charged Higgs signal efficiency for the four charged Higgs masses indicated on the figure from the process $pp \to t\bar{t}X$. This figure differs from the one shown in Fig. 9 in the minimum transverse momentum of the τ-jet, which is set to 20 GeV as opposed to 10 GeV used in the earlier figure

as well as the efficiency to tag two b-jets which is another factor of 2, and the efficiency of reconstructing a τ-jet, estimated as 0.3 [7]. This amounts to a factor of about 10 reduction in both the number of signal and background events, resulting in a significance of about 30. This is high enough to take another factor 2 reduction due to various other cuts, which will be inevitable in a detector-based analysis taking into account non-$t\bar{t}$ backgrounds, not estimated here. Of course, this significance goes down as m_{H^+} increases, keeping $\tan\beta$ fixed. Thus, for example, for $\tan\beta = 10$ and $m_{H^+} = 150$ GeV, the reduction in the number of events will be approximately 5 (a factor 10 decrease in $\mathcal{B}(t \to H^+ b)$, compensated by a factor 2 increase in the signal efficiency calculated from the BDTD response). This would yield $S \simeq 6$, which is just above the discovery limit for a charged Higgs below the top quark mass.

A number of checks has been performed in order to test the robustness of the results. For instance, the cut on the minimum transverse momentum of the τ-jet has been raised from 10 GeV to 20 GeV. The corresponding figure displaying the background rejection vs. the charged Higgs signal efficiency is shown in Fig. 10. A comparison with Fig. 8, obtained with a 10 GeV cut on the minimum transverse momentum of the τ-jet, shows that the two figures are very similar. The price to pay for the acceptance is, relatively speaking, minor, going down from 0.6 to 0.5. We had conservatively taken this to be 0.5 in our numerical calculations.

The above analysis presented for the LHC energy $\sqrt{s} = 14$ TeV has been repeated for a center of mass energy $\sqrt{s} = 7$ TeV, at which energy the LHC is collecting data currently. As of preparing this report, the integrated luminosity of the LHC is above 1 inverse femtobarn, and the projection for end 2012 is of order 10 inverse femtobarns. We have generated events at $\sqrt{s} = 7$ TeV, and have calculated all the distributions presented earlier for 14 TeV. The shapes of these distributions are essentially similar. This is reflected in the BDTD response functions for the SM background and the charged Higgs signal, presented in Fig. 11, and in the SM background rejection vs. the charged Higgs signal efficiency, shown in Fig. 12. However, the cross sections for $pp \to t\bar{t}X$ at 7 TeV is approximately a factor 4 smaller than at 14 TeV [35, 39]. This implies that our calculations for the significance obtained at $\sqrt{s} = 14$ TeV have to be divided by a factor 2 to get the corresponding significance at $\sqrt{s} = 7$ TeV. This will reduce the sensitivity of the charged Higgs in $\tan\beta$–m_{H^+} plane. For example, for m_{H^+} close to the kinematic limit $m_t - m_b$, a signal is expected only for $\tan\beta > 20$.

A potential dilution of the polarization information has to be kept in mind. The single charged-prong hadronic

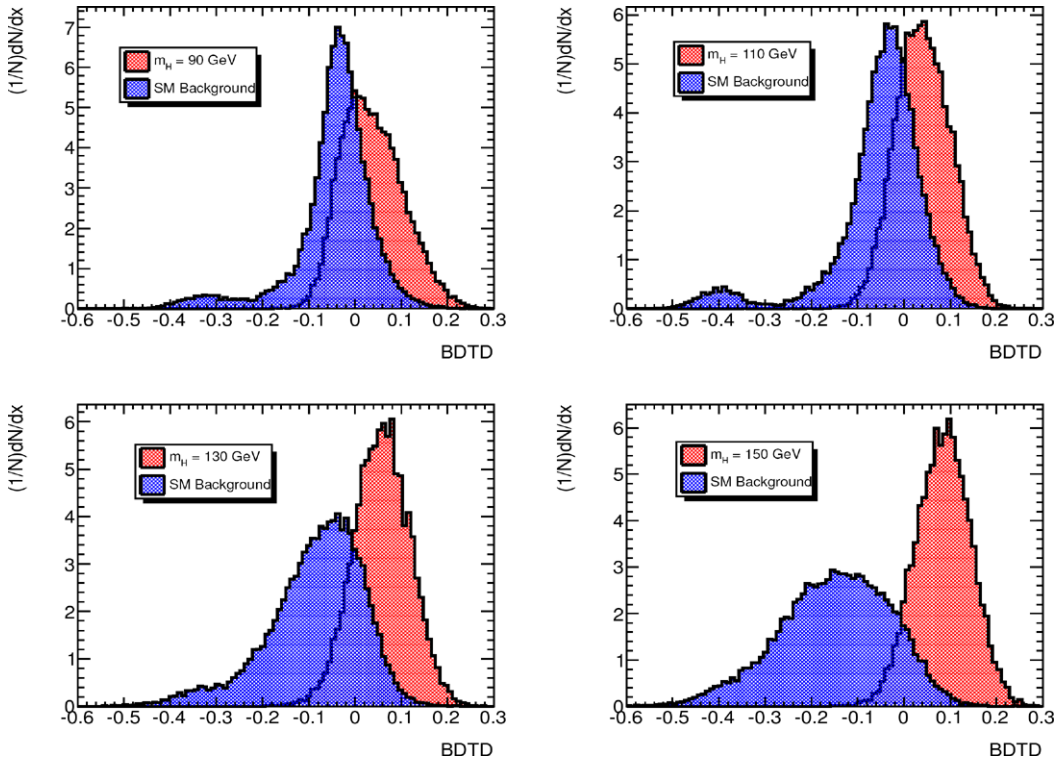

Fig. 11 (Color online) BDTD response functions for $pp \to t\bar{t}X$, with $\sqrt{s} = 7$ TeV, followed by the decay $t \to W^+b$ (SM) and the decay chain $t \to H^+b$, with the SM background (in *shaded blue*) and the charged Higgs signal process (in *shaded red*) for four different charged Higgs masses

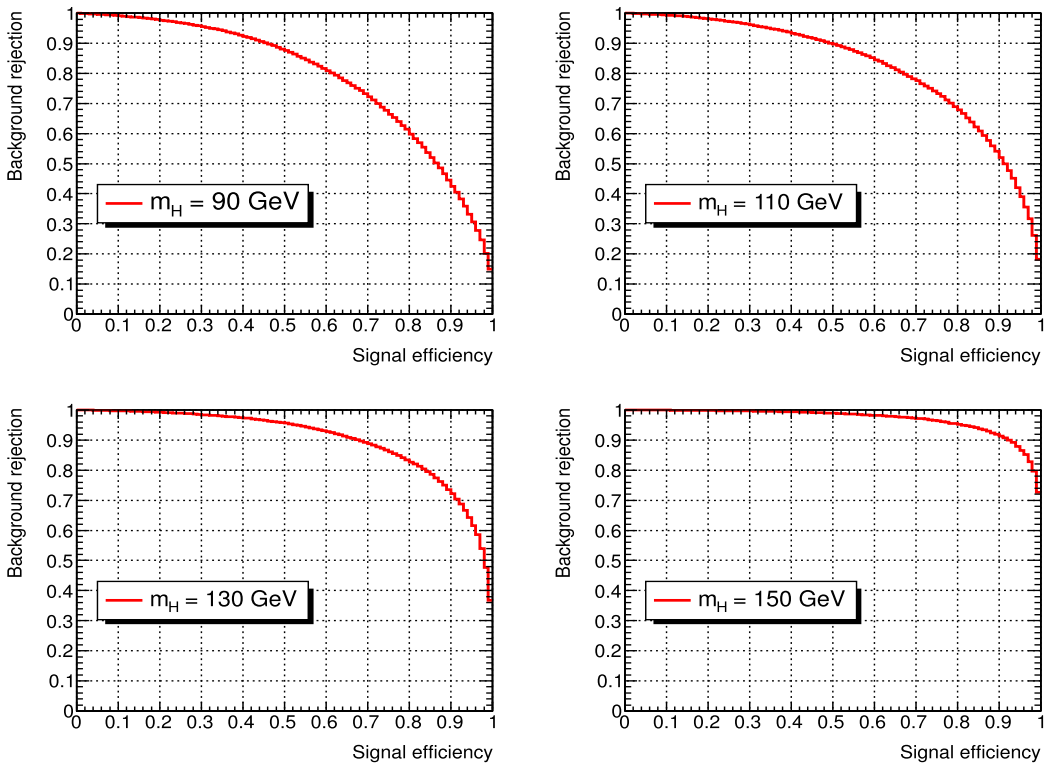

Fig. 12 (Color online) SM background rejection vs. charged Higgs signal efficiency for the four charged Higgs masses indicated on the figure from the process $pp \to t\bar{t}X$ with $\sqrt{s} = 7$ TeV

decays of the $\tau^{\pm}$ are essentially made up of the decays $\tau^{\pm} \to \pi^{\pm} + \nu_{\tau}$ (with a branching ratio of 10.9%), $\tau^{\pm} \to \rho^{\pm}(\to \pi^{\pm}\pi^0) + \nu_{\tau}$ decays (with a branching ratio of 25.5%) and $\tau^{\pm} \to a_1^{\pm}(\to \pi^{\pm}\pi^0\pi^0) + \nu_{\tau}$ decays (with a branching ratio of 9.3%). Separating the $\pi^{\pm}\nu_{\tau}$ mode from the $\rho^{\pm}\nu_{\tau}$ mode should, in principle, be possible due to the lack of deposited energy in the π^0 or electromagnetic cluster accompanying the $\pi^{\pm}$ in the former, but separating the $\rho^{\pm}\nu_{\tau}$ mode from the $a_1^{\pm}\nu_{\tau}$ mode will not be easy. Fortunately, the branching ratio of the latter is only 40% of the former. So, the number of π^0 clusters (0, 1 and 2) will have to be included in the analysis as a new variable. The $\tau^{\pm} \to \rho^{\pm}\nu_{\tau}$ decays dominate the one charged track ($\pi^{\pm}$, $K^{\pm}$) and one electromagnetic or π^0 cluster. However, we stress that the BDT can be trained to reduce the dilution.

In a realistic analysis, a further source of reduction in our estimates of the significance would come from the wrong assignment of the b-jet charges, though this effect is minor compared to the ones discussed above. The b-jet charge identification efficiency is estimated at present to be around 65% [7], using standard techniques based on a weighted average of the charges of the particles in the jet, with the weights being proportional to their momenta. However, a simple algorithm can be designed, which takes into account in addition the angular correlations between the trigger lepton, the tau-jet and the charges, reducing the b-jet misassignment to about 20% for the charged Higgs masses close to the $W^{\pm}$ mass. For higher charged Higgs masses, this can be further brought down by simply taking the b-jet with the smaller (larger) transverse momentum to be that associated with the charged Higgs (resp. $W^{\pm}$) boson.

We also mention that we have not considered the background from the process $pp \to t\bar{t} \to (b\ell\nu_{\ell})(bjj)$. However, it has been shown in [7] that this background can be well separated in a standard cut analysis from the $pp \to t\bar{t} \to (b\ell\nu_{\ell})(b\tau\nu_{\tau})$ process. With our TMVA approach, this background will be tamed though we will have to introduce also the missing E_T as a variable in the BDT training. We are aware of the non-$t\bar{t}$ background, which are dominated by the Z + jets and W + jets. These have been studied in great detail in [8], with the conclusion that they can be brought below the signal by the additional use of the $E_T^{\rm miss}$-cut. We have not used the $E_T^{\rm miss}$-cut, as we have concentrated only on the SM $t\bar{t}X$ background, but will do so in a more realistic detector-based analysis in the future.

3 Single $t/\bar{t}$ production and the decay chains $t \to bW^+/H^+ \to b(\tau^+\nu_{\tau})$ at the LHC

3.1 Cross sections at the LHC

The single top (or anti-top) cross sections in hadron collisions have been calculated in the NLO approximation [52–56]. Recalling that there are three basic processes at the leading order which contribute to $\sigma(p\bar{p} \to t/\bar{t}X)$, namely the t-channel: $qb \to q't$, the s-channel: $q\bar{q}' \to \bar{b}t$; and the associated tW production $bg \to tW^-$, the cross section estimated at the Tevatron is [57]: $\sigma(p\bar{p} \to tX) = \sigma(p\bar{p} \to \bar{t}X) \simeq 1.8$ pb for both the top and anti-top production. At the LHC@14 TeV, one estimates $\sigma(pp \to tX) \simeq 200$ pb and about half this number for $\sigma(pp \to \bar{t}X)$, yielding the summed single top and anti-top cross sections at about 300 pb, also approximately two orders of magnitude larger than those at the Tevatron. With a luminosity of 10 fb^{-1}, one anticipates $O(3 \times 10^6)$ single top (or anti-top) events.

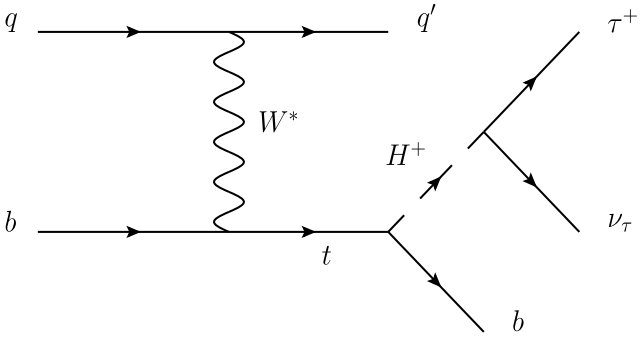

Fig. 13 Feynman diagram for $qb \to q't$, followed by the decay $t \to b(H^+ \to \tau^+\nu_{\tau})$

As mentioned in the introduction, there are three different mechanisms of producing a single top (or anti-top) quark in hadronic collisions, the s-channel, the t-channel, and the associated production tW-channel. The Feynman diagram for the dominant t-channel partonic process $qb \to q't$, followed by the decay $t \to b(H^+ \to \tau^+\nu_{\tau})$ is shown in Fig. 13. The partonic cross section is then convoluted with the parton distribution functions to calculate the cross sections in $pp \to t + X$ and $pp \to \bar{t} + X$. Since, we are using PYTHIA 6.4 [48] to do the simulation of the single top (or anti-top) production, not all channels are encoded there yet. However, as we use the generator to calculate the acceptance only, but the total cross sections are normalized to the theoretical calculations, the estimates presented here should hold approximately. Since most of the distributions calculated by us for the processes $pp \to t\bar{t}x$ and $pp \to t/\bar{t}X$ are in the same variables, we comment only briefly on the distributions for the signal $t \to bH^+ \to b\tau^+\nu_{\tau}$ and the background process $t \to bW^+ \to b\tau^+\nu_{\tau}$.

In Fig. 14, we show the distribution $dN/d\cos\psi$ for the $pp \to t/\bar{t} + X$ production as measured in the decay chain for the SM background process $t \to bW \to b(\tau\nu_{\tau}) \to b(\rho\bar{\nu}_{\tau})\nu_{\tau}$ (right-hand frame), and for the signal $t \to bH \to b(\tau\nu_{\tau}) \to b(\rho\bar{\nu}_{\tau})\nu_{\tau}$ (left-hand frame) for four different charged Higgs masses, as indicated on the figure. The SM background in the process $pp \to t/\bar{t} + X$ falls more steeply as a function of $\cos\psi$ than is the case for the $t\bar{t}$ production

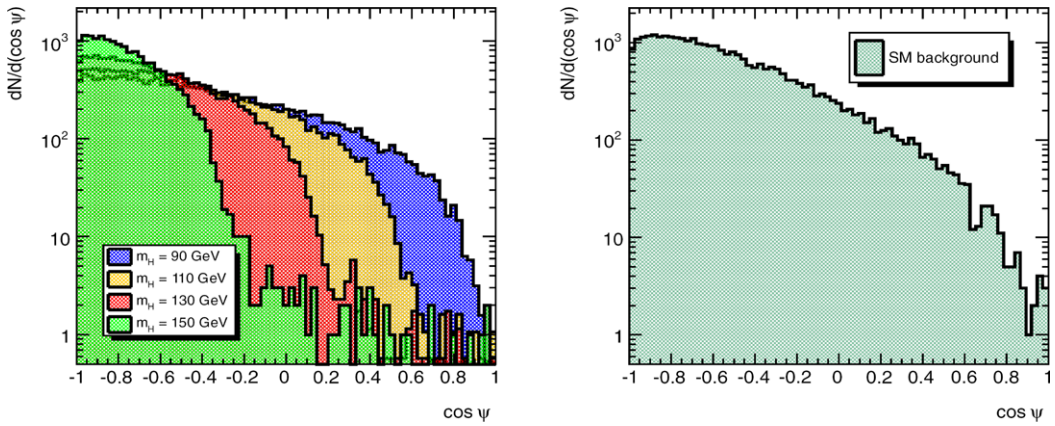

Fig. 14 (Color online) The distribution $dN/d\cos\psi$ for the $pp \to t/\bar{t} + X$ production as measured in the decay chain $t \to bW \to b(\tau\nu_\tau) \to b(\rho\bar{\nu}_\tau)\nu_\tau$ (*right-hand frame*), and in $t \to bH \to b(\tau\nu_\tau) \to b(\rho\bar{\nu}_\tau)\nu_\tau$ for four different charged Higgs masses, as indicated on the figure (*left-hand frame*)

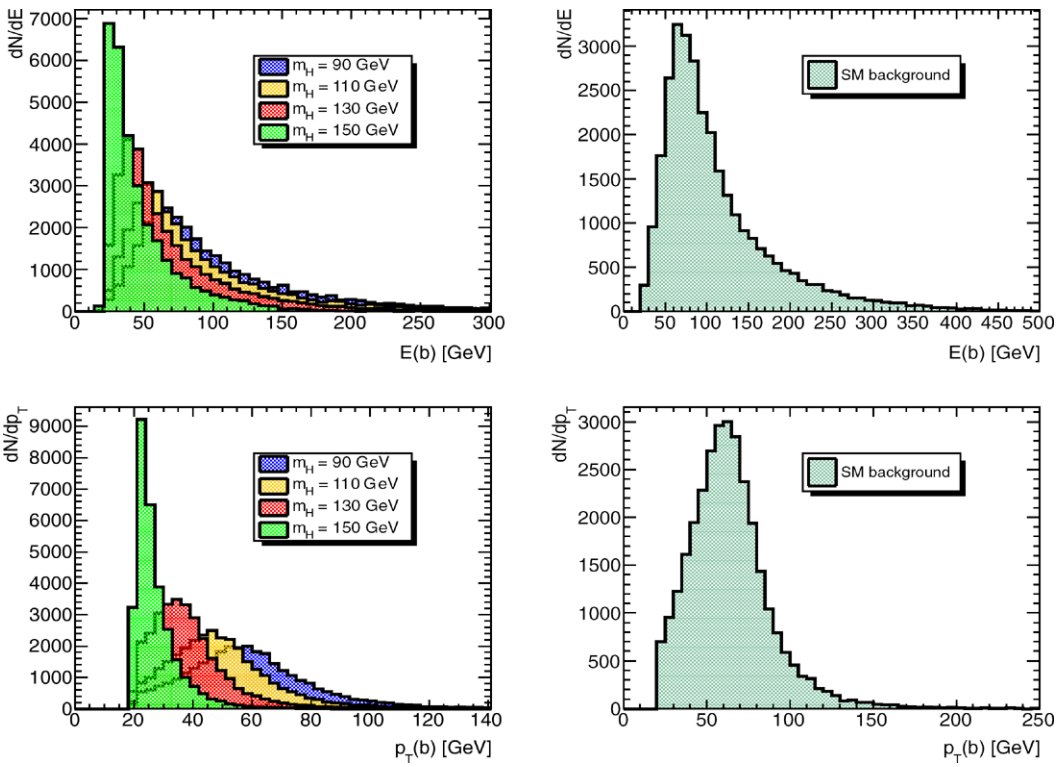

Fig. 15 (Color online) Distributions in the energy of the b-jet, $E(b)$, and transverse momentum of the b-jet, $p_T(b)$ from the process $pp \to t/\bar{t}X$, followed by the decay $t \to W^+b$ (*right-hand frames*), and the same distributions for the decay chain $t \to H^+b$ with the four indicated charged Higgs masses (*left-hand frame*)

$pp \to t\bar{t} + X$, due to the acceptance cuts. The trend is similar in the signal process. However, also in the single top (or anti-top) production, this distribution provides a good discriminant as input to the BDTD analysis.

The distributions in the energy of the b-jet, $E(b)$, and transverse momentum of the b-jet, $p_T(b)$ from the process $pp \to t/\bar{t}X$, followed by the SM decay $t \to W^+b$ are shown in Fig. 15 (right-hand frames), and the same distributions for the decay chain $t \to H^+b$ with the four indicated charged Higgs masses are also shown in this figure (left-hand frame). These distribution are very similar to the ones shown for the $pp \to t\bar{t}X$ processes, as they essentially reflect the kinematics of the decays $t \to W^+b$ and $t \to H^+b$.

In Fig. 16, we show the corresponding distributions for the τ-jet, $E(\tau\text{-jet})$, and for the transverse momentum of the τ-jet, $p_T(\tau\text{-jet})$ from the process $pp \to t/\bar{t}X$, followed by

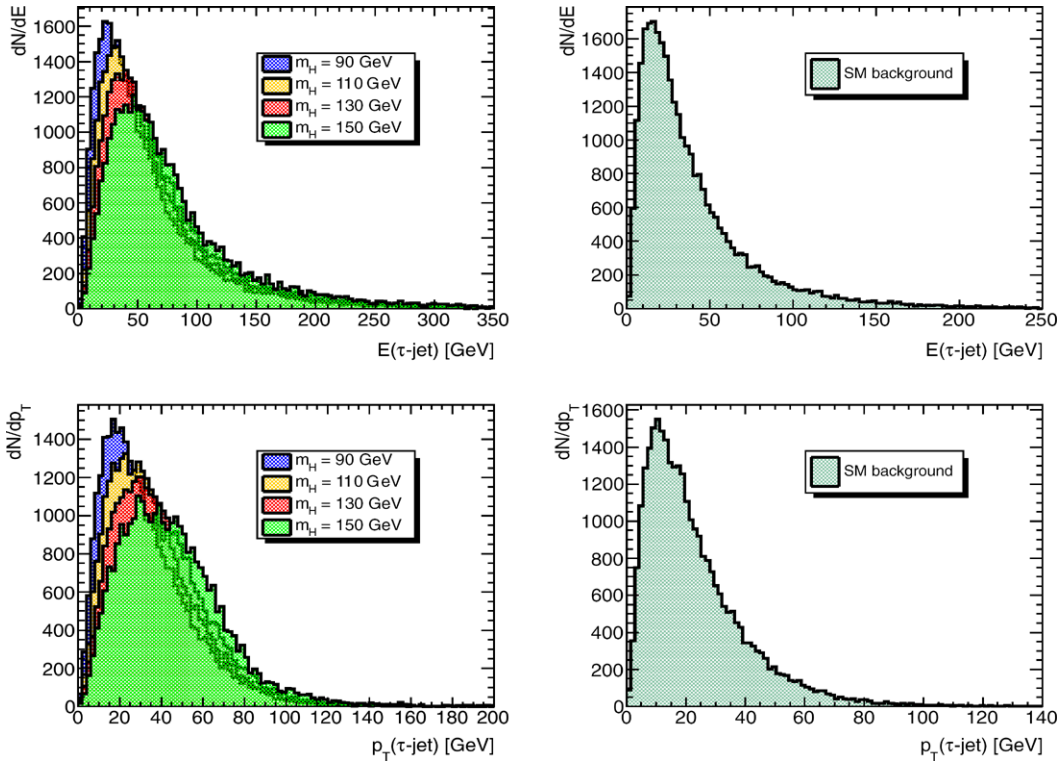

Fig. 16 (Color online) Distributions in the energy of the τ-jet, $E(\tau\text{-jet})$, and transverse momentum of the τ-jet, $p_T(\tau\text{-jet})$ from the process $pp \to t/\bar{t}X$, followed by the SM decay $t \to W^+b$ (*right-hand frames*), and the same distributions for the decay chain $t \to H^+b$ with the four indicated charged Higgs masses (*left-hand frame*)

the SM decay $t \to W^+b$ (right-hand frames), and the same distributions for the decay chain $t \to H^+b$ with the four indicated charged Higgs masses (left-hand frame). These distributions, likewise, are very similar to the ones shown for the $t\bar{t}$ production case, shown in the previous section.

The distributions in the ratio $E(\tau\text{-jet})/E(b)$ and $p_T(\tau\text{-jet})/p_T(b)$ from the process $pp \to t/\bar{t}X$, followed by the SM decay $t \to W^+b$ are shown in Fig. 17 (right-hand frames), and the same distributions for the decay chain $t \to H^+b$ are also shown in this figure with the four indicated charged Higgs masses (left-hand frame). As anticipated, these distributions are also similar in the single top (anti-top) production and in the $t\bar{t}$ production.

The effects of different chiralities in the SM decay chain $t \to bW^+ \to b(\tau^+\nu_\tau)$ followed by the τ^+ decay $\tau^+ \to \rho^+\bar{\nu}_\tau$, and in the signal process $t \to bH^+ \to b(\tau^+\nu_\tau)$ followed by the τ^+ decay $\tau^+ \to \rho^+\bar{\nu}_\tau$ are shown in Fig. 18. Once again, these distributions in the fractional energy of the single-charged prong (π^+ in τ^+-jet), $E(\pi)/E(\tau\text{-jet})$, and in the transverse momentum of the single-charged prong, $p_T(\pi)/p_T(\tau\text{-jet})$ are very similar in the processes $pp \to t/\bar{t}X$ and $pp \to t\bar{t}X$, as expected.

One important difference between the analysis of the single top (or anti-top) production compared to the $t\bar{t}$ production process lies in the fact that the missing transverse energy and momentum can be ascribed in the former to the τ-neutrino, ν_τ. This is different in the case of the $t\bar{t}$ production, as one of the t-or $\bar{t}$-quarks decays via $t \to bW^+ \to b\ell^+\nu_\ell$, which is used as a trigger. Thus, the missing transverse energy or momentum can not be traced to the decay of the τ-lepton alone in the case of $t\bar{t}$ production. As already stated in [30] the missing transverse energy and momentum profile in the case of the single top (or anti-top) process $pp \to t/\bar{t}X$ followed by $t \to bH^+ \to b\tau^+\nu_\tau$ can be used to constrain the mass of the charged Higgs. We pursue this idea, by using two different definitions of the transverse mass. In the first case, called $m_T^{(1)}$, this is defined as in [31]:

$$m_T^2 = 2p_T^\ell p_T^\nu (1 - \cos\phi_{\ell\nu}), \tag{13}$$

where p_T^ℓ, p_T^ν, and $\phi_{\ell\nu}$ are the momenta and angle between the leptons in the plane perpendicular to the pp collision axis. This definition was proposed to determine the transverse mass of the $W^\pm$ boson in $p\bar{p}$ collisions using the decay modes $W^\pm \to e^\pm\nu_e$ and $W^\pm \to \mu^\pm\nu_\mu$. In our case, where the charged Higgs decays via $H^+ \to \tau^+\nu_\tau$, the charged lepton is the τ^+, which is not measured experimentally. Since, we use the decay $\tau^+ \to \rho^+\bar{\nu}_\tau$, we replace the p_T^ℓ by the p_T of the ρ^+. The resulting $m_T^{(1)}$-distributions are shown in the upper two frames in Fig. 19 for the SM background (right-hand frame) and the charged Higgs case

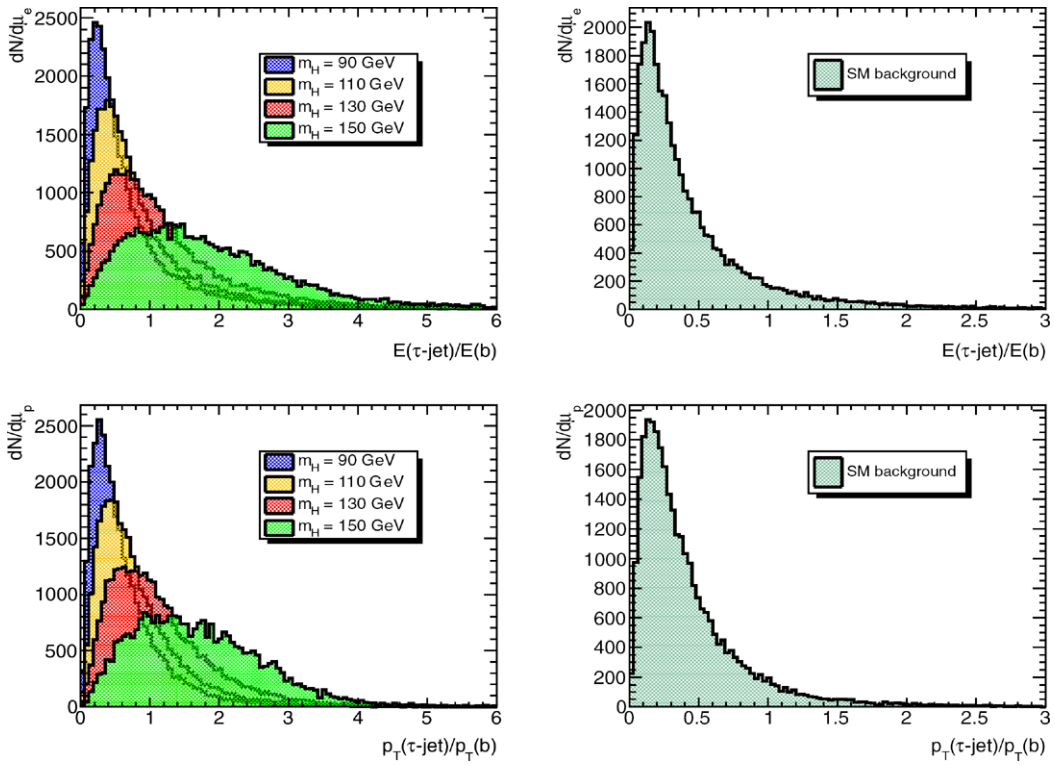

Fig. 17 (Color online) Distributions in the ratio $E(\tau\text{-jet})/E(b)$ and $p_T(\tau\text{-jet})/p_T(b)$ from the process $pp \to t/\bar{t}X$, followed by the SM decay $t \to W^+b$ (*right-hand frames*), and the same distributions for the decay chain $t \to H^+b$ with the four indicated charged Higgs masses (*left-hand frame*)

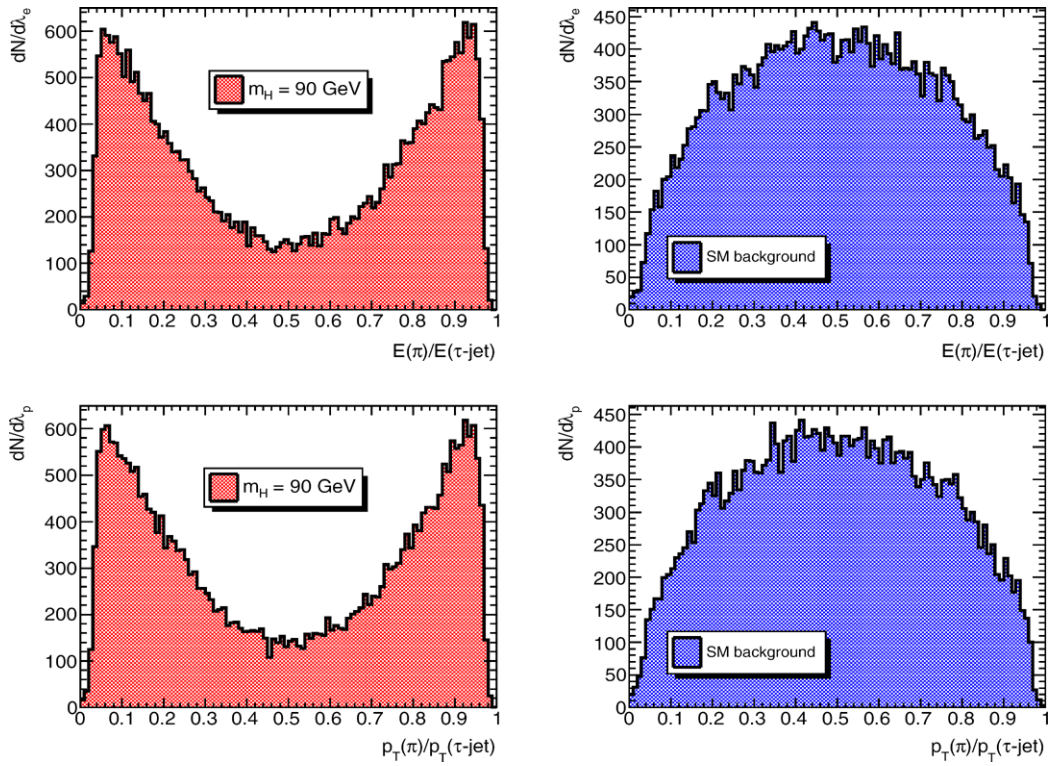

Fig. 18 (Color online) Distributions in the fractional energy of the single-charged prong (π^+ in τ^+-jet), $E(\pi)/E(\tau\text{-jet})$, and in the transverse momentum of the single-charged prong, $p_T(\pi)/p_T(\tau\text{-jet})$ from the $pp \to t/\bar{t}X$, followed by the SM decay $t \to W^+b$ (*right-hand frames*), and the same distributions for the decay chain $t \to H^+b$ with the four indicated charged Higgs masses (*left-hand frame*)

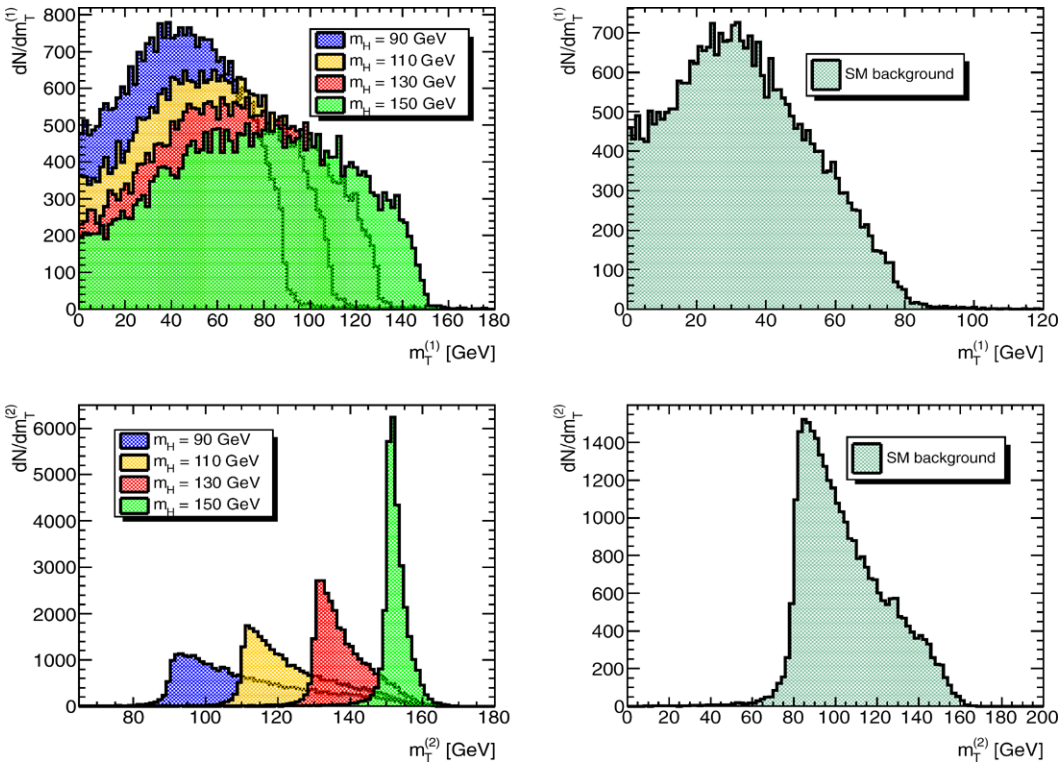

Fig. 19 (Color online) Transverse mass distributions for the $W^{\pm}$ in the process $pp \to t/\bar{t} + X$ followed by the decay $t \to bW^{+}$ (*right-hand frames*) and for the $H^{\pm}$ transverse mass for the decay chain $t \to H^{+}b$ with the four indicated charged Higgs masses (*left-hand frame*). The definitions used for defining the transverse masses $m_T^{(1)}$ and $m_T^{(2)}$ are given in the text

(left-hand frame). As seen from the distributions shown in the left-hand frame, this definition is not useful to see the Jacobian peak in the transverse mass of the $H^{\pm}$. This is anticipated since there are two undetected neutrinos from the $H^{\pm}$ vertex. The distributions in $m_T^{(1)}$ for the SM ($W^{\pm}$)-background and the $H^{\pm}$-signal are different, and they do add to the discriminating power in the BDTD analysis.

For the processes $pp(\bar{p}) \to t\bar{t}X$ and $pp(\bar{p}) \to t\bar{b}X$, with the subsequent decay of $t \to b(W^{+}, H^{+})$, if one of the two b jets could be associated with the semileptonic decay of the top quark, then the on-shell constraint for the top quark could be used in the form $(p^{\text{miss}} + p_\ell + p_b)^2 = m_{\text{t}}^2$. In this case, a transverse Higgs mass can be defined by maximizing the invariant mass, $(m_T^H)^2 = \max[(p_\ell + p^{\text{miss}})^2]$, since it is bounded from above by the top quark mass, with the charged Higgs transverse mass satisfying $m_{H^+} \le m_T^H \le m_{\text{t}}$, where m_{H^+} is the true charged Higgs mass. This leads to the following transverse mass definition for m_T^H [30], which we call $m_T^{(2)}$,

$$\left(m_T^H\right)^2 = \left(\sqrt{m_t^2 + \left(\vec{p}_T^{\,\ell} + \vec{p}_T^{\,b} + \vec{p}_T^{\,\text{miss}}\right)^2} - p_T^b\right)^2 - \left(\vec{p}_T^{\,\ell} + \vec{p}_T^{\,\text{miss}}\right)^2. \tag{14}$$

This expression holds by neglecting the b-quark mass. We have calculated the $m_T^{(2)}$ distributions, by replacing the $\vec{p}_T^{\,\ell}$ (which is $\vec{p}_T^{\,\tau}$ for our case) by $\vec{p}_T^{\,\rho}$. These distributions are shown in the lower two frames of Fig. 19, with the SM background (yielding the Jacobian peak of the $W^{\pm}$) shown on the right-hand frame, and the corresponding Jacobian peaks for the charged Higgs case, shown in the left-hand frame. For all the four charged Higgs masses shown in this frame, the Jacobian in $m_T^{(2)}$ has a sharp peak. Measuring these distributions provides, in principle, an estimate of $H^{\pm}$. We will use these distributions in $m_T^{(2)}$ to train our BDTD sample.

The distributions generated and discussed have been used to train the BDTD algorithms and the resulting response functions are shown in Fig. 20. The separation between the signal and the background improves as m_{H^+} increases, a trend which was also observed in the $pp \to t\bar{t}X$ production process.

The corresponding background rejection vs. signal efficiency curves from the processes $pp \to t/\bar{t}X$ calculated from the previous BDTD response at $\sqrt{s} = 14$ TeV are shown in Fig. 21 for the four charged Higgs masses, as indicated on the frames. For a signal efficiency value of 90%, the background rejection varies between 40% and 99% as we move from $m_{H^+} = 90$ GeV to $m_{H^+} = 150$ GeV.

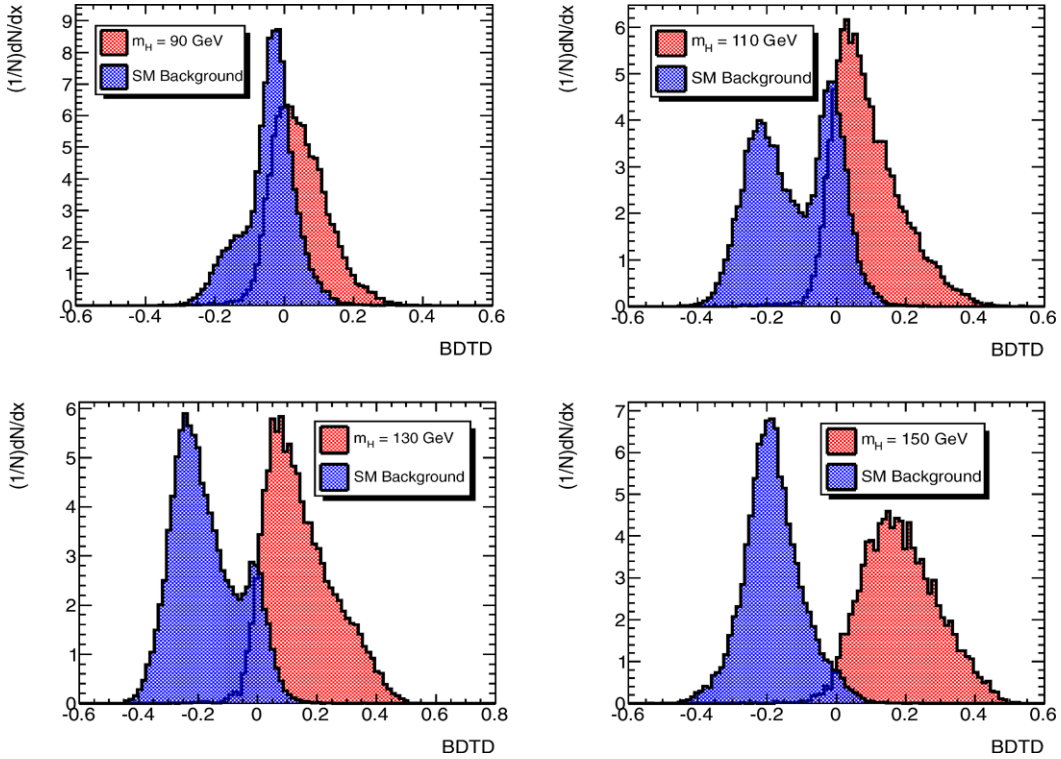

Fig. 20 (Color online) BDTD response functions for $pp \to t/\bar{t}X$, followed by the decay $t \to W^+b$ (SM) and the decay chain $t \to H^+b$, with the SM background (in *shaded blue*) and the charged Higgs signal process (in *shaded red*) for four different charged Higgs masses

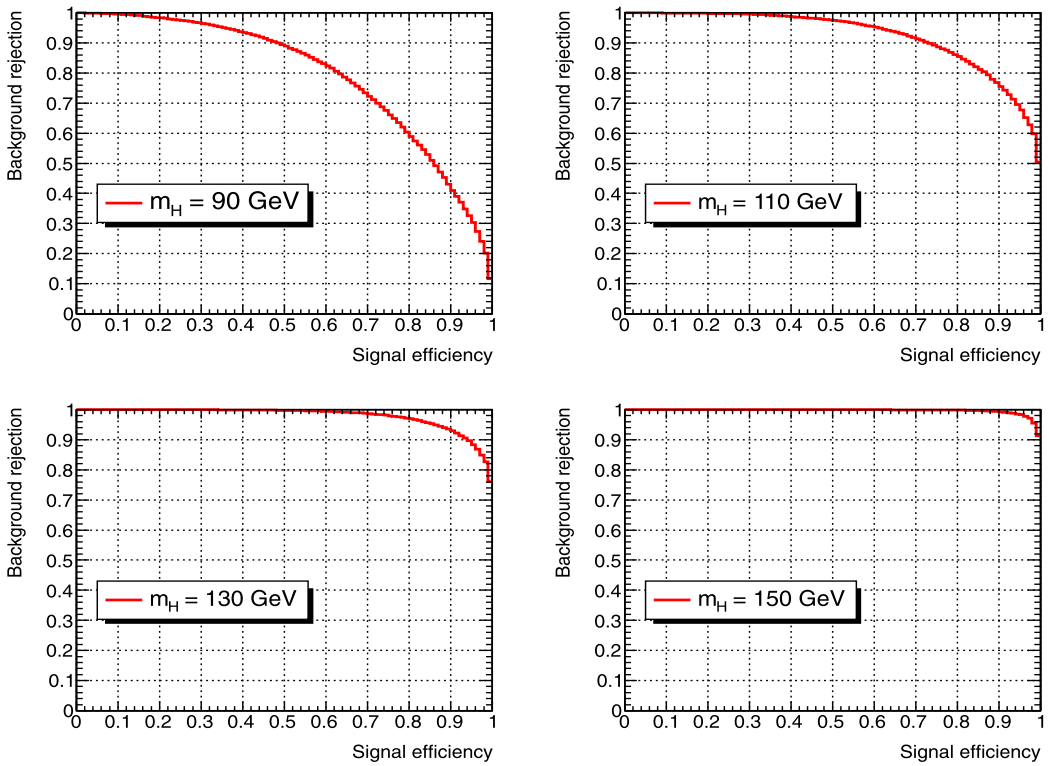

Fig. 21 (Color online) SM background rejection vs. charged Higgs signal efficiency for the four charged Higgs masses indicated on the figure from the process $pp \to t/\bar{t}X$

In order to calculate the significance of our signal, we do the following simplified calculation. We consider again the less preferred case for $\tan\beta = 10$, with $\mathcal{B}(t \to H^+ b) \simeq 0.02$ for $m_{H^+} = 90$ GeV. For the process $pp \to t/\bar{t}X$, our trigger is based on the τ-jet, coming from the decays $W^\pm/H^\pm \to \tau^\pm \nu_\tau$. Since, in the large-$\tan\beta$ limit we are working, $\mathcal{B}(H^+ \to \tau^+ \nu_\tau) \simeq 1$, and the τ^+-decay mode we are concentrating on is $\tau^+ \to \rho^+ \bar{\nu}_\tau$, which has a branching ratio of 0.25, the product branching ratio $t \to bH^+ \to b(\tau^+\nu_\tau) \to b(\rho^+\bar{\nu}_\tau)\nu_\tau = 5 \times 10^{-3}$, which is the same as in the case of top-quark pair production process $pp \to t\bar{t}X$. For an integrated luminosity of 10 $(\text{fb})^{-1}$, and inclusive single top cross section $\sigma(pp \to t/\bar{t}X = 300$ pb at $\sqrt{s} =$ 14 TeV, this yields 1.5×10^4 signal events. For the background events, resulting from the production and the SM decays from the process $pp \to t/\bar{t}X$, the corresponding product branching ratio is 2.5%, again the same as in the case of top-quark pair production process $pp \to t\bar{t}X$ yielding 7.5×10^4 background events. Using the BDTD analysis, we get for a 50% signal efficiency, a background rejection of 90%. Thus, our estimated significance will be

$$S = \frac{N_{\text{signal events}}}{\sqrt{N_{\text{background events}}}} = \frac{7.5 \times 10^3}{\sqrt{7.5 \times 10^3}} \simeq 85. \tag{15}$$

A more realistic calculation should consider a factor of 2 reduction due to the acceptance cuts, similar to those discussed in Sect. 2.3, as well as the efficiency to tag the b-jet, estimated as 70%, and the efficiency of reconstructing a τ-jet, estimated as 0.3. This amounts to a factor of about 10 reduction in both the number of signal and background events, resulting in a significance of about 25. Of course, this significance goes down as m_{H^+} increases, keeping $\tan\beta$ fixed. Thus, for example, for $\tan\beta = 10$ and $m_{H^+} = 150$ GeV, the reduction in the number of events will be approximately 5 (a factor 10 decrease in $\mathcal{B}(t \to H^+ b)$, compensated by a factor 2 increase in the signal efficiency calculated from the BDTD response). Since the background rejection goes up to 99%, this would yield $S \simeq 25$, allowing to search for a charged Higgs in the decay $t \to bH^+$, essentially up to a charged Higgs mass close to the kinematic limit.

We would like to stress that our philosophy in this paper is to show how to disentangle the process $pp \to t + X \to H^+ b + X$ from $pp \to t + X \to W^+ b + X$. In particular, single top production in hadron colliders is subject itself to backgrounds [7] which we have not considered here. The most relevant of these backgrounds is the $Wb\bar{b}$ production. Needless to say that the $\cos\psi$, the polarisation information on the $\tau^\pm$ from the decay $\tau^\pm \to \rho^\pm \nu_\tau$, and the transverse mass distribution will retain their discriminant power to suppress them, albeit at the cost of a small loss in the significance of the signal. We plan to take this into account together with a complete treatment of the detector effects in a forthcoming more realistic analysis, which is required to assign an error on the charged Higgs mass due to such effects.

4 Summary and outlook

We have reported here an analysis with improved sensitivity to charged Higgs searches in top quark decays $t \to bH^+ \to b\tau^+\nu_\tau$ at the LHC. We concentrate on hadronic $\tau^\pm$ decays, in particular, the decay mode $\tau^\pm \to \rho^\pm \nu_\tau$, and take into account the polarisation information of the $\tau^\pm$ passed on to $\rho^\pm$. The observables which play a dominant role in our analysis are the energy and p_T of the b-jets from the decays $t \to bW^+$ and $t \to bH^+$, energy and p_T of the $\tau^\pm$-jets from the two decay chains, and the energy and p_T of the single-charged prong ($\pi^\pm$ coming from the decay chain $\tau^\pm \to \rho^\pm \nu_\tau \to \pi^\pm \nu_\tau$). Distributions in these variables are studied together with angular distribution in $\cos\psi$ defined in (1). This information is fed to a multivariate analysis using the BDTD techniques. The BDTD response shows that a clear separation between the $t \to bW^+$ and $t \to bH^+$ decays can be achieved in both the $t\bar{t}X$ pair production and the $t/\bar{t}X$ single top production at the LHC. We have also shown that using a transverse mass definition, as suggested in [30], the process $pp \to t/\bar{t}X$ allows one to determine sharp Jacobian peaks for the mass of the $H^\pm$-bosons. With the benchmark integrated luminosity of 10 fb^{-1} at 14 TeV, the light charged Higgs ($m_{H^+} < m_t - m_b$) can be discovered for all values of $\tan\beta$, where the decay mode $H^\pm \to \tau^\pm \nu_\tau$ is dominant.

In estimating the quoted significances, we have assumed that the decay $t \to bW^+$ makes up the dominant background. This should be refined by taking into account non-t-backgrounds, such as coming from $(Z, W) +$ jets.

Acknowledgements We thank Merlin Kole, Theodota Lagouri and Torbjorn Sjostrand for helpful discussions. This research was partially supported by MICINN (Spain) under contract FPA2008-00601.

References

1. K. Nakamura et al. (Particle Data Group Collaboration), J. Phys. G **G37**, 075021 (2010)
2. M. Misiak et al., Phys. Rev. Lett. **98**, 022002 (2007). arXiv:hep-ph/0609232
3. T. Aaltonen et al. (CDF Collaboration), Phys. Rev. Lett. **103**, 101803 (2009). arXiv:0907.1269 [hep-ex]
4. For a recent update, see G. Bernardi, M. Carena, and T. Junk, Higgs Bosons: Theory and Searches, in the PDG review [1]
5. V.M. Abazov et al. (D0 Collaboration), Phys. Rev. D **80**, 051107 (2009). arXiv:0906.5326 [hep-ex]
6. O. Stal, arXiv:1012.2709 [hep-ph]
7. G. Aad et al. (The ATLAS Collaboration), arXiv:0901.0512 [hep-ex]
8. ATLAS Collaboration, ATLAS-NOTE ATL-PHYS-PUB-2010-006 (2010)

9. ATLAS Collaboration, ATLAS-NOTE ATL-PHYS-PUB-2010-003 (2010)
10. G.L. Bayatian et al. (CMS Collaboration), J. Phys. G **34**, 995 (2007)
11. M. Baarmand, M. Hashemi, A. Nikitenko, J. Phys. G **32**, N21 (2006)
12. R. Kinnunen, PoS **CHARGED2008**, 007 (2008)
13. K. Hagiwara, A.D. Martin, D. Zeppenfeld, Phys. Lett. B **235**, 198 (1990)
14. B.K. Bullock, K. Hagiwara, A.D. Martin, Phys. Rev. Lett. **67**, 3055 (1991)
15. A. Rouge, Z. Phys. C **48**, 75 (1990)
16. B.K. Bullock, K. Hagiwara, A.D. Martin, Nucl. Phys. B **395**, 499 (1993)
17. D.P. Roy, Phys. Lett. B **277**, 183 (1992)
18. S. Raychaudhuri, D.P. Roy, Phys. Rev. D **52**, 1556 (1995). arXiv:hep-ph/9503251
19. S. Raychaudhuri, D.P. Roy, Phys. Rev. D **53**, 4902 (1996). arXiv:hep-ph/9507388
20. D.P. Roy, Phys. Lett. B **459**, 607 (1999). arXiv:hep-ph/9905542
21. K.A. Assamagan, Y. Coadou, Acta Phys. Pol. B **33**, 707 (2002)
22. Q.H. Cao, S. Kanemura, C.P. Yuan, Phys. Rev. D **69**, 075008 (2004). arXiv:hep-ph/0311083
23. A. Ali, E.A. Kuraev, Y.M. Bystritskiy, Eur. Phys. J. C **67**, 377 (2010). arXiv:0911.3027 [hep-ph]
24. D. Eriksson, G. Ingelman, J. Rathsman, O. Stal, J. High Energy Phys. **0801**, 024 (2008). arXiv:0710.5906 [hep-ph]
25. J. Han, M. Kamber, *Data Mining Concepts and Techniques* (Elsevier, Amsterdam, 2006)
26. V.M. Abazov et al. (D0 Collaboration), Phys. Rev. Lett. **103**, 092001 (2009). arXiv:0903.0850 [hep-ex]
27. T. Aaltonen et al. (CDF Collaboration), Phys. Rev. Lett. **103**, 092002 (2009). arXiv:0903.0885 [hep-ex]
28. Z. Liu, FERMILAB-THESIS-2009-45
29. A. Ali, F. Barreiro, T. Lagouri, Phys. Lett. **B693**, 44–51 (2010). arXiv:1005.4647 [hep-ph]
30. E. Gross, O. Vitells, Phys. Rev. **D81**, 055010 (2010). arXiv:0907.5367 [hep-ph]
31. J. Smith, W.L. van Neerven, J.A.M. Vermaseren, Phys. Rev. Lett. **50**, 1738 (1983)
32. S. Hesselbach, S. Moretti, J. Rathsman, A. Sopczak, Eur. Phys. J. C **53**, 311 (2008). arXiv:0708.4394 [hep-ph]
33. R. Bonciani, S. Catani, M.L. Mangano, P. Nason, Nucl. Phys. B **529**, 424 (1998). Erratum-ibid. B **803**, 234 (2008). arXiv:hep-ph/9801375
34. M. Cacciari, S. Frixione, M.L. Mangano, P. Nason, G. Ridolfi, J. High Energy Phys. **0809**, 127 (2008). arXiv:0804.2800 [hep-ph]
35. N. Kidonakis, R. Vogt, Phys. Rev. D **78**, 074005 (2008). arXiv:0805.3844 [hep-ph]
36. S. Moch, P. Uwer, Phys. Rev. D **78**, 034003 (2008). arXiv:0804.1476 [hep-ph]
37. A.D. Martin, W.J. Stirling, R.S. Thorne, G. Watt, Phys. Lett. B **652**, 292 (2007). arXiv:0706.0459 [hep-ph]
38. P.M. Nadolsky et al., Phys. Rev. D **78**, 013004 (2008). arXiv:0802.0007 [hep-ph]
39. U. Langenfeld, S. Moch, P. Uwer, arXiv:0907.2527 [hep-ph]
40. A. Czarnecki, S. Davidson, Phys. Rev. D **47**, 3063 (1993). arXiv:hep-ph/9208240
41. A. Czarnecki, S. Davidson, Phys. Rev. D **48**, 4183 (1993). arXiv:hep-ph/9301237
42. C.S. Li, T.C. Yuan, Phys. Rev. D **42**, 3088 (1990). Erratum-ibid. D **47**, 2156 (1993)
43. J. Guasch, R.A. Jimenez, J. Sola, Phys. Lett. B **360**, 47 (1995). arXiv:hep-ph/9507461
44. J.A. Coarasa Perez, D. Garcia, J. Guasch, R.A. Jimenez, J. Sola, Eur. Phys. J. C **2**, 373 (1998). arXiv:hep-ph/9607485
45. M.S. Carena, D. Garcia, U. Nierste, C.E.M. Wagner, Nucl. Phys. B **577**, 88 (2000). arXiv:hep-ph/9912516
46. T. Hahn, S. Heinemeyer, W. Hollik, H. Rzehak, G. Weiglein, Nucl. Phys. Proc. Suppl. **183**, 202 (2008)
47. A. Sopczak, PoS **CHARGED2008**, 023 (2008). arXiv:0907.1498 [hep-ph]
48. T. Sjostrand, S. Mrenna, P.Z. Skands, J. High Energy Phys. **0605**, 026 (2006). hep-ph/0603175
49. S. Jadach, Z. Was, R. Decker, J.H. Kühn, Comput. Phys. Commun. **76**, 361 (1993)
50. A. Höcker et al., PoS A **CAT**, 040 (2007). arXiv:physics/0703039
51. S. Heinemeyer, W. Hollik, G. Weiglein, Comput. Phys. Commun. **124**, 76–89 (2000). hep-ph/9812320
52. B.W. Harris, E. Laenen, L. Phaf, Z. Sullivan, S. Weinzierl, Phys. Rev. D **66**, 054024 (2002). arXiv:hep-ph/0207055
53. N. Kidonakis, Phys. Rev. D **74**, 114012 (2006). arXiv:hep-ph/0609287
54. Q.H. Cao, R. Schwienhorst, C.P. Yuan, Phys. Rev. D **71**, 054023 (2005). arXiv:hep-ph/0409040
55. S. Heim, Q.H. Cao, R. Schwienhorst, C.P. Yuan, Phys. Rev. D **81**, 034005 (2010). arXiv:0911.0620 [hep-ph]
56. N. Kidonakis, Phys. Rev. D **75**, 071501 (2007). arXiv:hep-ph/0701080
57. N. Kidonakis, Nucl. Phys. A **827**, 448C (2009). arXiv:0901.2155 [hep-ph]